Stability of Nonlinear Convection-Diffusion-Reaction Systems in Discontinuous Galerkin Methods

C. Michoski[ϒ⋆†], A. Alexanderian[†¶], C. Paillet[*], E.J. Kubatko[‡], C. Dawson[†]

Aerospace Engineering Sciences, Computational Mechanics and Geometry Laboratory (CMGLab)[⋆]
University of Colorado at Boulder, Boulder, CO 80302,
Institute for Computational Engineering and Sciences (ICES)[†]
University of Texas at Austin, Austin, TX 78712,
Department of Mathematics[¶]
North Carolina State University, Raleigh, NC, 27695
Civil Engineering and Geodetic Engineering Department[‡]
The Ohio State University, Columbus, OH 43210
Department of Mechanical Engineering[*], École normale supérieure de Cachan, Cachan, France 94230

Abstract

In this work we provide an extension of the classical von Neumann stability analysis for high-order accurate discontinuous Galerkin methods applied to generalized nonlinear convection-reaction-diffusion systems. We provide a partial linearization under which a sufficient condition emerges that guarantees stability in this context. The stability behavior of these systems is then closely analyzed relative to Runge-Kutta Chebyshev (RKC) and strong stability preserving (RKSSP) temporal discretizations over a nonlinear system of reactive compressible gases arising in the study of atmospheric chemistry.

1 Introduction

In numerical methods, stability analysis is an essential tool for understanding and controlling the behavior of equation systems. Generally stability analysis can be applied to implicit or explicit timestepping methods, where the notions of both absolute and relative stability have been well-characterized [21]. The absolute stability region of a method can be determined from the region where the amplification factor of the method is bounded above by unity, while the relative stability is a more nuanced concept requiring an understanding of specific aspects of the solution itself, leading to the concept of, for example, order stars [46], which not only characterize stability of the method, but also limitations on its accuracy.

In explicit timestepping methods, two often complementary ways of approaching the temporal stability of a particular evolving system of equations is by way of either identifying the relevant CFL condition, or alternatively, by determining the von Neumann stability constraints as determined from the region of absolute stability; where, in the simplest of cases, the two can be shown to

[ϒ] Corresponding author, *michoski@gmail.com*

coincide. It is, however, also frequently the case that the von Neumann stability timestepping constraint is more strict than the derived CFL-type constraint [42].

The von Neumann stability analysis, in particular, has been applied in broad contexts for developing an understanding of how the characteristic eigenstructure of a particular system can be used to predict and preserve the stability behavior of a numerical method. These techniques have been extended to high-order accurate models and primarily developed and analyzed in the context of linear hyperbolic conservation laws [12, 17, 19, 20]. The goal of this work is to extend the classical von Neumann analysis to support generalized nonlinear convection-reaction-diffusion equations discretized via high-order accurate discontinuous Galerkin methods.

We start by considering a generic equation of the form $\boldsymbol{u}_t - \mathcal{L} = 0$, where $\mathcal{L}$ is a nonlinear differential operator. In the case where $\mathcal{L}$ is linear and hyperbolic the situation is fairly well-understood in the numerical setting (see for example [17, 19] in the case of scalar transport), and total variation diminishing schemes such as strong stability preserving schemes are often very effective at recovering linear stability of the solution to a fixed order of accuracy. However, when $\mathcal{L}$ is a nonlinear operator that includes nonlinear reactive/source terms, nonlinear convection terms, as well as nonlinear diffusion terms, the situation can be more complicated.

In this present work, we consider initial-boundary value problems that can be broadly written as a system of nonlinear convection-diffusion-reaction equations, of the form,

$$\begin{aligned} &\partial_t u_j(x,t) = \mathcal{L}_j(\partial_x^2 \boldsymbol{u}(x,t), \partial_x \boldsymbol{u}(x,t), \boldsymbol{u}(x,t), t), \quad (x,t) \in \Omega \times (0,T),\ j = 1,\dots,N, \\ &\boldsymbol{u}(x,0) = \boldsymbol{u}_0, \quad (x,t) \in \Omega, \\ &\boldsymbol{u}(x,t) = \boldsymbol{u}_b \quad (x,t) \in \partial\Omega \times (0,T). \end{aligned} \tag{1.1}$$

Here $\boldsymbol{u} = (u_1, \dots, u_N)^\top$ is the state vector, and the physical domain $\Omega \subset \mathbb{R}$ is an open bounded interval. An intuitive way of thinking about (1.1) is by decomposing the nonlinear operator into its component parts, such that:

$$\boldsymbol{u}_t = \mathcal{L}_{\mathscr{R}} + \mathcal{L}_{\mathscr{D}} + \mathcal{L}_{\mathscr{C}}, \quad \forall t \in (0,T) \tag{1.2}$$

where $\mathcal{L}_{\mathscr{R}} = \mathcal{L}_{\mathscr{R}}(\boldsymbol{u})$, $\mathcal{L}_{\mathscr{D}} = \mathcal{L}_{\mathscr{D}}(\boldsymbol{u}, \boldsymbol{u}_x, \boldsymbol{u}_{xx})$, and $\mathcal{L}_{\mathscr{C}} = \mathcal{L}_{\mathscr{C}}(\boldsymbol{u}, \boldsymbol{u}_x)$ are reactive, and divergence form diffusive and convective operators, respectively. In this work these operators correspond to the mathematical concepts of nonlinear subsystems of ODEs (i.e. the reactive subsystem), parabolic-like PDEs (i.e. the diffusion subsystems), and hyperbolic-like PDEs (i.e. the convection subsystems). It is important to recognize that the nonlinearity in these subsystems tends to lead to dynamics that are not purely hyperbolic (or parabolic), etc.

The basic behavior of the pure subsystems (i.e. of type reactive, parabolic, and hyperbolic) is reasonably well-characterized in comparison to the nonlinear mixed equation (1.2). For example, parabolic subsystems of the form $\boldsymbol{u}_t = \mathcal{L}_{\mathscr{D}}$ are known to be rather stiff numerically, and to produce highly stringent CFL-type timestepping restrictions. Similarly reactive subsystems can be reduced to nonlinear first-order ordinary differential equations $\boldsymbol{u}_t = \mathcal{L}_{\mathscr{R}}$, where the Jacobian matrix of this operator has indeterminate spectrum (in contrast to purely hyperbolic and parabolic operators, which are always real-valued), and is also often characterized by numerical stiffness.

It is, however, not infrequently the case in nonlinear application models that convection-diffusion-reaction systems are treated as dominated (and as a consequence completely determined) by one of these "pure-form" solutions, viz. convection-dominated flows being treated as purely "hyperbolic systems." Though this can be both a convenient as well as important simplifying assumption, it

can also, when done without completely determining the full impact of the subordinate subsystem (for example, the parabolic subsystem in a convection-dominated flow), lead to unexpected and unpredictable stability behavior. For example, in concert with parabolic subsystems, coupled reaction-diffusion can readily lead, in even simple cases, to traveling wave-form solutions (e.g. shockwave-type structures with zero wavespeed [34]), demonstrating locally varying spectrum (see for example the Poincare-Lyapunov Theorem), and even nonintegrable solution behavior [27].

Thus, while it can be tempting to view these three subsystems as distinct, and while it can even be done explicitly (e.g. numerically up to a formal "splitting error") by way of a fractional multistep operator splitting method [8, 16, 30, 36], it is important to note that it is often the interactions between the three subsystems that ultimately characterize the signature model behavior of the coupled problem, and thus determine the stability properties of the flow. This interacting aspect of nonlinearly-coupled subsystems can lead to dynamics that can show very different behaviors than that of the pure subsystems they are comprised of. However, just as importantly, this is also not always the case, in that coupled subsystems can also be truly dominated by one of the pure subsystems to such an extent that neglecting contributions from the subordinate dynamics can, under certain circumstances, be absolutely essential to fully optimizing performance.

This nuanced, and delicate, solution behavior is perhaps underscored by the broad array of application models subsumed by the system of equations (1.2). Indeed the purview of applications described under the general description of nonlinear systems of convection-diffusion-reaction equations is remarkably vast. For example, many standard models in continuum mechanics fit within this designation, including: multicomponent reactive Navier-Stokes [39], two-fluid plasma [24], MHD [37], and reduced plasma fluid models [10], shallow water equations [7], morphodynamics [18], first order acoustics and scattering [40], Maxwell's equations in classical electrodynamics [1], and so forth. However, the scope of convection-diffusion-reaction systems is not restricted to classical continuum models, but extends to statistical representations as well, such as those frequently used in biological [25, 45] and chemical applications [27]. The scope of these systems even extends to full phase space dynamics, such as those encoded by the Fokker-Planck [22] and Vlasov-Poisson [14] equations, which themselves span fields ranging from the molecular description of fluids, plasmas, and gases [6, 11, 15], to the collective behavior of aggregates with individual agency, as demonstrated in models arising in sociology and economics [29], etc.

Though nonlinear convection-diffusion-reaction equation are quite common, the classical von Neumann stability analysis is not, in the standard sense, directly applicable to such nonlinear problems. In practice, the lack of rigorous stability results in such cases, can lead practitioners to approximate CFL-type conditions derived for complicated models using relatively simple heuristic arguments. Indeed, these heuristics can fail to provide the strict estimates desired for *guaranteeing* global stability. In this paper, we present a systematic approach for generalizing a von Neumann-like stability analysis in the context of nonlinear convection-diffusion-reaction systems of the form (1.2), that have been spatially discretized using discontinuous Galerkin methods. In particular, we develop a systematic procedure that can be used in concert with the DG spatial discretization to partially linearize any equation of the form (1.2), such that nonlinear stability conditions can be computed, and ultimately used to determine lower bounds on the necessary timestep size dt needed to guarantee stability of the method. Throughout our numerical tests, we examine both the explicit Runge-Kutta Chebyshev (RKC) and strong stability preserving (RKSSP) temporal discretizations, and illustrate their different behaviors relative to different physical regimes.

It should be further noted here that the lack of CFL inequalities, and/or von Neumann stability

estimates on the timestep in these nonlinear problems, should not be taken as an indication that additional forms of temporal stability are not known, and of substantial practical importance. For example, as discussed in our previous work [27], fractional multistepping can be performed outright up to "splitting error," where the split form of the operators can then be solved using mixed IMEX (implicit/explicit) type methods [31] and/or implicit Integration Factor (IF) methods [23], for example. When these methods are applied linear stability results follow due, in part, to implicit time integration in "stiff" terms with fixed order splitting assumptions, etc. The forms of stability that follow, such as A-stable, C-stable, and L-stable methods, require additional assumptions on the linearity of the operator $\mathcal{L}_j$, even when the sign of the operator is "indefinite" [31]. In this paper, we do not perform operator splitting, or for that matter make additional constraints on the nonlinearity of the operators of the subsystems (or the signs of their eigenvalues), but rather develop a framework to determine lower bounds on the necessary timestep size dt needed to preserve nonlinear stability of an explicit timestepping method assuming a potentially highly nonlinear dynamics with indeterminant nonlinear coupling. In other words, the framework developed here can also be used to determine whether operator splitting, and/or implicit timestepping, might be necessary given a nonlinear system of equations. In this sense, the results in this paper can be viewed as a guide for developing a deeper analytic framework around the numerical behavior of nonlinear systems of equations discretized using discontinuous Galerkin methods.

The paper begins in Section 2.1 by introducing the discontinuous Galerkin spatial discretization, where the standard approximation spaces are reviewed. In Section 2.2 the variational form of (1.2) is derived in full, where the details of this derivation become important for the development of the stability results to follow. In Section 2.3 the temporal discretization procedures are discussed, where in this paper we restrict to two basic temporal discretization methods: the RKSSP and the RKC schemes. Section 3 is dedicated to the main stability theorem of the paper. In Section 3.1 we show how a partial linearization of the system is enough to reformulate the problem into a form that is fully amenable to classical-type von Neumann stability analysis. In Section 3.2 the von Neumann analysis is performed on the system, which follows immediately from Section 3.1. Finally, in Section 3.3 we present a nonlinear stability theorem, predicated on a discrete nonlinear stability condition. This theorem is enough to guarantee stability in nonlinear convection-diffusion-reaction systems 1.2. Section 5.1 characterizes a physical problem arising in atmospheric chemistry. This problem utilizes a reduced form of the reactive multicomponent Navier-Stokes equations, where some of the basic mathematical properties of this system are discussed. In Section 5 the basic numerical behavior of the system from Section 5.1 is presented, and some of the relevant physical regimes are discussed. Finally, in Section 5.2 the stability of these nonlinear systems is evaluated closely, where multiple numerical experiments are performed, along with insight and discussion about their meaning and relationship to both the physical and theoretical aspects of the system. In Section 6 we conclude, and discuss some remaining open problems and future directions.

2 Discretization Schemes

In this Section we discuss the discretization schemes used throughout the paper. The discontinuous Galerkin method is used for the spatial discretization, which is then utilized to recast the system (1.2) into its variational form. The temporal discretizations used in this paper are the classical strong stability preserving Runge-Kutta schemes (RKSSP) and the "optimal thin region stability" preserving, Runge-Kutta Chebyshev (RKC) schemes.

2.1 Spatial Discretization in Classical Discontinuous Galerkin Methods

Consider a bounded open interval $\Omega \subset \mathbb{R}$ with boundary $\partial\Omega = \Gamma$, and given $T > 0$, we let $\mathcal{Q}_T = ((0,T) \times \Omega)$. Let Ω_h denote the partition of the discretization of Ω into a finite number of subintervals $\Omega_{e_1}, \Omega_{e_2}, \ldots, \Omega_{e_\ell}$. Here we define the mesh width h, and let Γ_{ij} denote the boundary shared by two neighboring elements Ω_{e_i} and Ω_{e_j}. Finally let $\Xi(i)$ denote the indexing set spanning the left and right shared boundary of each element Ω_{e_i}, such that $\partial\Omega_{e_i} = \bigcup_{j\in\Xi(i)} \Gamma_{ij}$.

We are interested in obtaining an approximate solution to u at time t on the finite dimensional space of discontinuous piecewise polynomial functions over Ω restricted to $\mathscr{T}_h$, given as

$$S_h^p(\Omega_h, \mathscr{T}_h) = \{v : v_{|\Omega_{e_i}} \in \mathscr{P}^p(\Omega_{e_i}), \quad \forall \Omega_{e_i} \in \mathscr{T}_h\}$$

where $\mathscr{P}^p(\Omega_{e_i})$ the space of polynomials of degree less than or equal to p defined on Ω_{e_i}.

Choosing a set of degree p polynomial basis functions $N_l \in \mathscr{P}^p(\mathcal{G}_i)$ for $l = 0, \ldots, n_p$ the corresponding degrees of freedom in the nodal basis, we can denote the state vector at time t over Ω_h, by

$$u_h(x,t) = \sum_{l=0}^{n_p} u_h^i(x_l^i, t) N_l^i(x), \quad \forall x \in \Omega_{e_i},$$

where N_l^i are the finite element shape functions, and u_l^i correspond to the nodal coordinates. The finite dimensional test functions φ_h are characterized by

$$\varphi_h(x) = \sum_{l=0}^{n_p} \varphi_l^i N_l^i(x), \quad \forall x \in \Omega_{e_i},$$

where φ_ℓ^i are the nodal values of the test functions in each Ω_{e_i}. It should be noted that all computations below follow through choosing a modal basis as well.

2.2 Variational Form of the System

Using the definitions from Section 2.1 we can recast (1.1) into a local variational form[1]:

$$\begin{aligned}\frac{d}{dt}\int_{\Omega_{e_i}} \varphi_h u_j(x,t)\,dx &= \int_{\Omega_{e_i}} \varphi_h \mathcal{L}_j(\partial_x^k u(x,t), u(x,t), t)\,dx \\ &= \int_{\Omega_{e_i}} \varphi_h \mathcal{L}_{\mathscr{R}j}(u(x,t),t)\,dx + \int_{\Omega_{e_i}} \varphi_h \mathcal{L}_{\mathscr{D}j}(\partial_x^2 u(x,t),t)\,dx \\ &\quad + \int_{\Omega_{e_i}} \varphi_h \mathcal{L}_{\mathscr{C}j}(\partial_x u(x,t), u(x,t), t)\,dx,\end{aligned} \tag{2.1}$$

where φ_h is chosen as a test function. We proceed by linearizing (1.1) in the mixed form, by defining the j auxiliary variables

$$\sigma_j(x,t) = \partial_x u_j(x,t), \tag{2.2}$$

[1]Note that here we choose the weak mixed formulation for convenience, but the resulting theory can be easily shown to work more broadly, e.g. the strong form mixed formulation.

such that we can rewrite (2.1) as

$$\begin{aligned}\frac{d}{dt}\int_{\Omega_{e_i}}\varphi_h u_j(x,t)\,dx = &\int_{\Omega_{e_i}}\varphi_h\mathcal{L}_{\mathscr{R}j}(u(x,t),t)\,dx + \int_{\Omega_{e_i}}\varphi_h\mathcal{L}_{\mathscr{D}j}(\partial_x\sigma(x,t),t)\,dx \\ &+ \int_{\Omega_{e_i}}\varphi_h\mathcal{L}_{\mathscr{C}j}(\partial_x u(x,t),u(x,t),t)\,dx,\end{aligned} \tag{2.3}$$

and the auxiliary weak form of (2.2) satisfies

$$\int_{\Omega_{e_i}}\varphi_h\sigma_j(x,t)\,dx = \int_{\Omega_{e_i}}\partial_x(\varphi_h u_j(x,t))\,dx - \int_{\Omega_{e_i}}u_j(x,t)\partial_x\varphi_h\,dx. \tag{2.4}$$

The standard discrete approximations follow in each term of (2.1), where we only draw attention to the convection and diffusion terms. First the convection term is integrated by parts to recover the interelement fluxes. That is, componentwise we can write

$$\int_{\Omega_{e_i}}\varphi_h\mathcal{L}_{\mathscr{C}j}(\partial_x u(x,t),u(x,t),t)\,dx = \int_{\Omega_{e_i}}\partial_x(\varphi_h f_j(u(x,t))\,dx - \int_{\Omega_{e_i}}f_j(u(x,t))\partial_x\varphi_h\,dx,$$

where the convective numerical flux $\hat{F}_{i\ell}$ will be represented by,

$$F_{ij} := \sum_{\ell\in\Xi(i)}\int_{\Gamma_{i\ell}}\hat{F}_{i\ell}(u_h|_{\Gamma_{i\ell}},u_h|_{\Gamma_{\ell i}},n_{i\ell})\varphi_h|_{\Gamma_{i\ell}}dS \approx \int_{\partial\Omega_{e_i}}\varphi_h f_j(u(x,t)ndS. \tag{2.5}$$

Here n_{ij} is the unit outward normal to $\partial\Omega_{e_i}$ on $\Gamma_{i\ell}$, while $\varphi_{|\Gamma_{i\ell}}$ and $\varphi_{|\Gamma_{\ell i}}$ denote the values of φ on $\Gamma_{\ell j}$ considered from the interior and the exterior of Ω_{e_i}, respectively. Here and below we will choose $\hat{F}_{i\ell}$ from the usual class of monotone numerical fluxes. Notice that the form of (2.5) presumes an indeterminate function f satisfying $\mathcal{L}_{\mathscr{C}j}(\partial_x u(x,t),u(x,t),t) = \partial_x f_j$.

Similarly, the diffusive flux is integrated by parts,

$$\begin{aligned}\int_{\Omega_{e_i}}\varphi_h\mathcal{L}_{\mathscr{D}j}(\partial_x u(x,t),u(x,t),t)\,dx = &\int_{\Omega_{e_i}}\partial_x(\varphi_h g_j(\sigma(x,t),u(x,t)))\,dx \\ &- \int_{\Omega_{e_i}}g_j(\sigma(x,t),u(x,t))\partial_x\varphi_h\,dx,\end{aligned} \tag{2.6}$$

where the diffusive flux $\hat{G}_{i\ell}$ is characterized by

$$G_{ij} := \sum_{\ell\in\Xi(i)}\int_{\Gamma_{i\ell}}\hat{G}_{i\ell}(\sigma_h|_{\Gamma_{i\ell}},\sigma_h|_{\Gamma_{\ell i}},u_h|_{\Gamma_{i\ell}},u_h|_{\Gamma_{\ell i}},n_{i\ell})\varphi_h|_{\Gamma_{ij}}dS \approx \int_{\partial\Omega_{e_i}}\varphi_h g_j(\sigma(x,t),u(x,t))ndS.$$

As above, we again assume some indeterminate function g, such that $\mathcal{L}_{\mathscr{D}j}(\partial_x u(x,t),u(x,t),t) = \partial_x g$.

The exact numerical form, as so determined by a choice of flux, will ultimately be chosen from the broad class of unified fluxes [2, 3]. Finally, in the usual way as above, the auxiliary flux $\hat{X}_{i\ell}$ is represented by:

$$X_{ij} := \sum_{\ell\in\Xi(i)}\int_{\Gamma_{i\ell}}\hat{X}_{i\ell}(u_h|_{\Gamma_{i\ell}},u_h|_{\Gamma_{\ell i}},n_{i\ell})\varphi_h|_{\Gamma_{i\ell}}dS \approx \int_{\Omega_{e_i}}\partial_x(\varphi_h u(x,t))\,dx.$$

Using the above for each species j we can now write the semidiscrete form of (1.2) as

$$\begin{aligned}\frac{d}{dt}\int_{\Omega_{e_i}}\varphi_h u_j^h\,dx &= \int_{\Omega_{e_i}}\varphi_h\mathcal{L}_{\mathscr{R}j}(u_h,t)\,dx + F_{ij} + G_{ij}\\ &\quad -\int_{\Omega_{e_i}} f_j(u_h)\partial_x\varphi_h\,dx - \int_{\Omega_{e_i}} g_j(\sigma_h,u_h)\partial_x\varphi_h\,dx,\\ \int_{\Omega_{e_i}}\varphi_h\sigma_j^h\,dx &= X_{ij} - \int_{\Omega_{e_i}} u_j^h\partial_x\varphi_h\,dx.\end{aligned} \tag{2.7}$$

2.3 Temporal Discretization: RKSSP and RKC

In this section, we describe the time discretization schemes for the semi-discrete version of (1.1),

$$\mathbf{M}\boldsymbol{u}_t^h = \mathcal{L}\big(\boldsymbol{u}^h(t)\big), \tag{2.8}$$

where $\mathbf{M}$ is the mass matrix associated to the finite element spatial discretization of (1.1). Below we briefly discuss the Runge-Kutta schemes for time integration of the system.

RKSSP schemes: Consider a system of the form

$$u_t = \mathcal{L}(u).$$

Here we describe the family of SSP (strong stability preserving) Runge-Kutta schemes, as discussed in [32, 33], and as originally designed for hyperbolic type problems [13]. We denote a generalized s stage of order γ SSP Runge-Kutta method by RKSSP(s,γ). The RKSSP(s, γ) can be written in the following form:

$$\begin{aligned}&u^{(0)} = u^n,\\ &u^{(i)} = \sum_{r=0}^{i-1}\left(\alpha_{ir}u^r + \Delta t\beta_{ir}\mathcal{L}^r\right), \quad \text{for } \ i = 1,\dots,s\\ &u^{n+1} = u^{(s)}.\end{aligned}$$

Here α_{ir} and β_{ir} are coefficients, $\mathcal{L}^r = \mathcal{L}(u^r, t^n + \delta_r\Delta t)$ and the solution at the nth timestep is given as $u^n = u_{|t=t^n}$ and at the $(n+1)$-st timestep by $u^{n+1} = u_{|t=t^{n+1}}$, with $t^{n+1} = t^n + \Delta t$. The second argument in $\mathcal{L}^r$ corresponds to the time-lag. That is $\delta_r = \sum_{l=0}^{r-1}\mu_{rl}$, where $\mu_{ir} = \beta_{ir} + \sum_{l=r+1}^{i-1}\mu_{lr}\alpha_{il}$, where we have taken that $\alpha_{ir} \geq 0$ satisfying $\sum_{r=0}^{i-1}\alpha_{ir} = 1$.

RKC schemes: To recover the so-called "optimal thin region stability" (see [41, 44]) originally designed for parabolic type problems [43], we alternatively adopt the finite damped χ-staged Runge-Kutta Chebyshev (RKC) method of second order, which can be written as follows:

$$\begin{aligned}&u^{(0)} = u^n,\\ &u^{(1)} = u^{(0)} + \Delta t^n\tilde{\mu}_1\mathcal{L}^0,\\ &u^{(j)} = (1-\hat{\mu}_j-\hat{\nu}_j)\,u^{(0)} + \hat{\mu}_j u^{(j-1)} + \hat{\nu}_j u^{(j-2)} + \Delta t^n\tilde{\mu}_j\mathcal{L}^{j-1} + \Delta t^n\tilde{\gamma}_j\mathcal{L}^0, \quad \text{for } j\in\{2,\dots,\chi\},\\ &u^{n+1} = u^{(\chi)}.\end{aligned}$$

Here, $\tilde{\mu}_1 = \omega_1\omega_0^{-1}$ and for each $j \in \{2,\dots,\chi\}$:

$$\hat{\mu}_j = \frac{2\hat{b}_j\omega_0}{\hat{b}_{j-1}}, \quad \hat{\nu}_j = \frac{-\hat{b}_j}{\hat{b}_{j-2}}, \quad \tilde{\mu}_j = \frac{2\hat{b}_j\omega_1}{\hat{b}_{j-1}} \quad \tilde{\gamma}_j = -a_{j-1}\tilde{\mu}_j,$$
$$\text{where} \quad a_j = 1 - b_jT_j(\omega_0), \quad \hat{b}_0 = \hat{b}_2, \quad \hat{b}_1 = \omega_0^{-1} \quad \hat{b}_j = T_j''(\omega_0)T_j'(\omega_0)^{-2}, \quad \text{for} \quad j \in \{2,\dots,\chi\},$$
$$\text{with } \omega_0 = 1 + \epsilon\chi^{-2}, \quad \omega_1 = T_\chi'(\omega_0)T_\chi''(\omega_0)^{-1},$$

where the T_j are the Chebyshev polynomials of the first kind, and U_j the Chebyshev polynomials of the second kind which define the derivatives, given by the recursion relations:

$$T_0(x) = 1, \quad T_1(x) = x, \qquad T_j(x) = 2xT_{j-1}(x) - T_{j-2}(x) \quad \text{for} \quad j \in \{2,\dots,\chi\},$$
$$U_0(x) = 1, \quad U_1(x) = 2x, \quad U_j(x) = 2xU_{j-1}(x) - U_{j-2}(x) \quad \text{for} \quad j \in \{2,\dots,\chi\},$$
$$T_j'(x) = jU_{j-1}, \quad T_j''(x) = \left(j\frac{(j+1)T_j - U_j}{x^2-1}\right) \quad \text{for} \quad j \in \{2,\dots,\chi\}.$$

Finally the operator $\mathcal{L}^j$ is evaluated at time $\mathcal{L}^j(t^n + \tilde{c}_j\Delta t^n)$, where the $\tilde{c}_j$ are given by:

$$c_0 = 0, \quad c_1 = \tfrac{1}{4}c_2\omega_0^{-1}, \quad c_j = \frac{T_\chi'(\omega_0)T_j''(\omega_0)}{T_\chi''(\omega_0)T_j'(\omega_0)} \approx \frac{j^2-1}{\chi^2-1} \quad \text{for } j \in \{2,\dots,\chi-1\}, \quad c_\chi = 1.$$

Since we consider only second order RKC methods, in what follows, we denote by RKC(s) an s-stage RKC scheme.

Traditionally, stability of RK schemes is studied through linear stability analysis where one considers the linear ODE $u_t = \lambda u$. The stability region of an RK scheme is obtained by considering the corresponding characteristic polynomial (also referred to as the stability polynomial), $P(z)$, with $z = \Delta t\,\lambda$, given by

$$S_{\text{stab}} = \{z \in \mathbb{C} : |P(z)| \le 1\}.$$

For the purposes of illustration, in the top row of Fig. 1, we show the stability regions of second order RKSSP and RKC schemes evaluated at different stages. In the bottom row of Fig. 1, we show the dependence of the stability region of RKC(5) on the parameter ϵ. Notice that as $\epsilon \to \infty$, we recover the stability region of the RKSSP(2,5).

Note that in the case of a linear system of the form $\boldsymbol{u}_t = L\boldsymbol{u}$, with the state vector $\boldsymbol{u}(t) \in \mathbb{R}^n$ and $L \in \mathbb{R}^{n\times n}$, one conventionally studies the stability region of the method by considering the eigenvalues of L. More generally, for a nonlinear system, $\boldsymbol{u}_t = F(\boldsymbol{u})$, with $\boldsymbol{u} : \mathbb{R}_+ \to V \subset \mathbb{R}^n$, to ensure stability, we consider the set

$$E = \{\Delta t\lambda : \lambda \text{ is an eigenvalue of } J_{\boldsymbol{u}}F(\boldsymbol{u}), \mathrm{Re}(\lambda) \le 0, \boldsymbol{u} \in V\},$$

and require that $E \subset S_{\text{stab}}$; see e.g., [41] for more details. In the present work, we study the stability of the RK schemes for fully coupled nonlinear systems of type (1.1). More precisely, we study the stability of the semi-discrete system (2.8), where the right hand side operator is given by the spatial discretization of a nonlinear system of PDEs. In our study we use an approach motivated by a classical von Neumann analysis (see e.g., [38]), and the approach taken in [17, 19] as discussed in detail in Section 3.

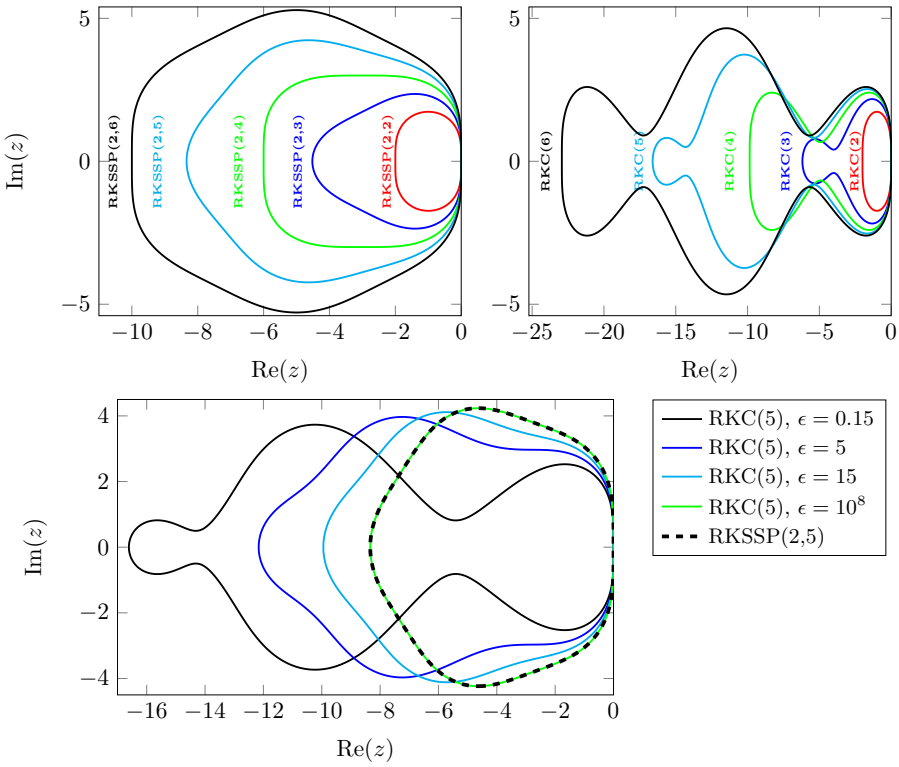

Figure 1: Top row: the stability regions for RKSSP(2, s) and RKC(s) with stages $s = 3, \ldots, 6$. The RKC schemes use $\epsilon = 0.15$. Bottom row: the effect of the parameter ϵ on the stability region of the RKC(5) scheme.

3 A Framework for Stability Analysis in Nonlinear Systems

The strategy for developing a framework for the stability analysis will be in keeping with a generalized approach to the classical von Neumann stability analysis. The approach will be to partially linearize the operator $\mathcal{L}$, and study the stability theory as a local signature of the nonlinear system. Once the Fourier components of the partially linearized operator are recovered, a simple transformation of the form of the equation allows the proof of a nonlinear stability theorem for convection-diffusion-reaction systems of the form (1.2).

3.1 Partial Linearization of the Operators

Here we will restrict to the Legendre polynomial basis, denoted by $\{\varphi_l\}_{l=1}^{n_p}$, for the test space. Note that this choice is relatively arbitrary, and the following analysis remains valid for any orthogonal basis. Recall that the Legendre polynomials satisfy $\int_{-1}^{1} \varphi_l \varphi_m = 2/(2l+1)\delta_{lm}$ for $l, m \in \{1, \ldots, n_p\}$. Using the orthogonality of the basis, and setting u_{jl}^i to mean the lth degree of freedom of the jth species component on the ith element, we can rewrite (2.7) in terms of a single nodal component l,

as

$$\begin{aligned}\frac{d}{dt}u^i_{jl}(t) =& \frac{2l+1}{h}\Big\{ \int_{\Omega_{e_i}} \varphi_l(x)\mathcal{L}_{\mathscr{R}j}(u_h,t)\,dx + F_{ijl} + G_{ijl} \\ &- \int_{\Omega_{e_i}} f_j(u_h)\partial_x\varphi_l(x)\,dx - \int_{\Omega_{e_i}} g_j(\sigma_h,u_h)\partial_x\varphi_l(x)\,dx\Big\}.\end{aligned} \tag{3.1}$$

The goal now is to factor the coefficients of u through the nonlinear system. Towards this, we make use of the following basic partial linearization assumptions on the first order variation in the Taylor series expansion of the fluxes:

$$f_j(u_h) \approx (J_u f_j)u^h_j, \quad \mathcal{L}_{\mathscr{R}j}(u_h) \approx (J_u\mathcal{L}_{\mathscr{R}j})u^h_j, \quad \text{and} \quad g_j(\sigma_h,u_h) \approx (J_{\nabla u}g_j)\sigma_j, \tag{3.2}$$

where the notation used for these Jacobian products is explained/defined below.

To arrive at these partial linearizations, one must use a Taylor series expansion about a point, and restrict to the first order variation. For example, consider the convective flux f:

$$f(u_h) \approx f(u_0) + Jf(u_0)(u_h - u_0)$$

The linearization point u_0 is eventually taken as the previous timestep $u_0 = u^{n-1}$. The above relation also satisfies

$$f(u_h) \approx (Jf)u_h + b,$$

where b does not depend on u_h. In the context of stability analysis we will be focusing on the linear part, $\tilde{f}(u_h) \approx (Jf)u_h$, where $\tilde{f}(u_h)$ is an isometry preserving the first order variation. As a result we drop the tilde, and notice that what is meant by the jth entry of $f(u_h)$ is

$$f_j(u_h) \approx (J_u f_j)u^h_j,$$

where j is the species index, making $(J_u f_j)u^h_j$ the jth entry in the matrix-vector multiplication $(Jf)u_h$. Notice that this notation should be understood as,

$$(J_u f_j)u^h_j := \Big((J_u f)u^h\Big)_j = \sum_k (J_u f)_{jk}u^h_k = \left(\sum_k (J_u f)_{jk}\frac{u^h_k}{u^h_j}\right)u^h_j, \tag{3.3}$$

where the last equality assumes $u^h_j > 0$, though note that this assumption is never actually needed in the actual computation described in Section 3.2. This is because here we have written the terms "componentwise" to connect with the standard theoretical presentation [20], though when actually computing these terms, we naturally sum over the component index j first, making the Jacobian factorization trivial. The other two terms in (3.2) follow in a very similar way.

Using these approximations, the convective flux term (2.5) is now able to be linearly decomposed into a contribution from a base Ω_{e_i} and neighboring Ω_{e_ℓ} elements over each node l:

$$\begin{aligned}F_{ijl} &\approx \int_{\partial\Omega_{e_i}} (J_u f_j)u^h_j\varphi_l n dS \\ &\approx \sum_{\ell\in\Xi(i)} \int_{\Gamma_{i\ell}} F_{ij\ell}(u_h|_{\Gamma_{i\ell}}, u_h|_{\Gamma_{\ell i}}, n_{i\ell})u^h_j|_{\Gamma_{i\ell}}\varphi_l|_{\Gamma_{i\ell}} dS.\end{aligned}$$

For simplicity, we choose $F_{ij\ell}$ using a classical monotone flux, so that it linearly depends on the stencil and can clearly be split over the base element component and the neighboring element component in terms of some indeterminant F' (up to the exact choice of numerical flux), such that

$$\sum_{\ell\in\Xi(i)}\int_{\Gamma_{i\ell}} F_{ij\ell}(u_h|_{\Gamma_{i\ell}},u_h|_{\Gamma_{\ell i}},n_{i\ell})u_j^h|_{\Gamma_{i\ell}}\varphi_l|_{\Gamma_{i\ell}}dS = \left(\sum_{k,m}^{n_p} F'_{jkm}u_m\varphi_l\right)\Big|_{\Gamma_{i\ell}} + \left(\sum_{k,m}^{n_p} F'_{jkm}u_m\varphi_l\right)\Big|_{\Gamma_{\ell i}}. \tag{3.4}$$

Note that k, m, and l all span the nodal degrees of freedom here, and thus F'_{jkm} is an $N\times(n_p+1)\times(n_p+1)$ tensor. Using this notation as well as (3.2) we can recast (3.1) as

$$\begin{aligned}\frac{d}{dt}u_{jl}^i =& \frac{2l+1}{h}\Bigg\{\int_{\Omega_{e_i}}\varphi_l(J_u\mathcal{L}_{\mathscr{R}j})u_j^h\,dx + \left(\sum_{k,m}^{n_p} F'_{jkm}u_m\varphi_l\right)\Big|_{\Gamma_{i\ell}} + \left(\sum_{k,m}^{n_p} F'_{jkm}u_m\varphi_l\right)\Big|_{\Gamma_{\ell i}}\\ &+ G_{ijl} - \int_{\Omega_{e_i}}(J_u f_j)u_j^h\partial_x\varphi_l\,dx - \int_{\Omega_{e_i}} g_j(\sigma_k^h,u_h)\partial_x\varphi_l\,dx\Bigg\}.\end{aligned} \tag{3.5}$$

Notice that all that has been done here is that numerical fluxes have been split into components relative to element ownership. So, for example, the different contributions from these fluxes, such as classical jump terms, are seen simply by summing over species index j and nodal index l:

$$\begin{aligned}\int_{\partial\Omega_i}[\![u_h^i]\!]\varphi_h n dS &= \int_{\partial\Omega_i}(u_h^i|_{\Gamma_{i\ell}} - u_h^i|_{\Gamma_{\ell i}})\varphi_h n dS\\ &= \left(\sum_{k,m}^{n_p} F'_{km}u_m\varphi_h\right)\Big|_{\Gamma_{i\ell}} + \left(\sum_{k,m}^{n_p} F'_{km}u_m\varphi_h\right)\Big|_{\Gamma_{\ell i}},\end{aligned}$$

where the F''s would all be unity in this simple case, and so forth.

It remains to factor the diffusive terms G_{ijl}. These terms follow in a very similar way to the convective flux terms F_{ijl}, except for now we have to factor through the two separate fluxes that linearize the second order operator; namely the diffusive flux G_{ijl}, and the auxiliary flux X_{ijl}. Towards this end notice that (2.4) factors through the diffusive fluxes, where first

$$\sigma_j(t) = M_j^{-1}\left(\int_{\partial\Omega_{e_i}}\varphi_h u_j^h n dS - \int_{\Omega_{e_i}} u_j^h\partial_x\varphi_h\,dx\right).$$

Note that here M_j is the diagonal (species-wise) DG mass matrix. Using the same technique as for the convective flux above, this term can be rewritten in each node l over the local stencil, as

$$\sigma_{jl} = \frac{2l+1}{h}\left(\left[\sum_k^{n_p} X'_{jk}u_k\varphi_l\right]\Big|_{\Gamma_{i\ell}} + \left[\sum_k^{n_p} X'_{jk}u_k\varphi_l\right]\Big|_{\Gamma_{\ell i}} - \int_{\Omega_{e_i}} u_j^h\partial_x\varphi_l\,dx\right). \tag{3.6}$$

The diffusive fluxes are now written in terms of these factored σ_{jl}'s, such that we have

$$\begin{aligned} G_{ijl} &\approx \int_{\partial\Omega_{e_i}} \varphi_l g_j(\sigma,u) n dS \\ &\approx \int_{\partial\Omega_{e_i}} \varphi_l (J_{\nabla u} g_j)\sigma_j n dS \\ &\approx \int_{\partial\Omega_{e_i}} \varphi_l \sum_{k,m}^{n_p} [J_{\nabla u} g_j]_{km}\sigma_{jk} n dS \\ &\approx \sum_{\ell\in\Xi(i)} \int_{\Gamma_{i\ell}} G_{ij\ell}(\sigma_h|_{\Gamma_{i\ell}}, \sigma_h|_{\Gamma_{\ell i}}, u_h|_{\Gamma_{i\ell}}, u_h|_{\Gamma_{\ell i}}, n_{i\ell})\sigma_j^h|_{\Gamma_{ij}}\varphi_l|_{\Gamma_{ij}} dS. \end{aligned} \tag{3.7}$$

The crucial observation here, is that σ_j^h in (3.7) is determined by (3.6), so that the edge diffusive term in (3.9) demonstrates a domain of dependence that is two layers of elements thick from the base element Ω_{e_i}. That is, since the factored σ_{jl} depends on a local stencil of elements (3.6), the G's, as determined in the same way as the F's,

$$\begin{aligned} \sum_{\ell\in\Xi(i)} \int_{\Gamma_{i\ell}} & G_{ij\ell}(\sigma_h|_{\Gamma_{i\ell}},\sigma_h|_{\Gamma_{\ell i}}, u_h|_{\Gamma_{i\ell}}, u_h|_{\Gamma_{\ell i}}, n_{i\ell})\sigma_j^h|_{\Gamma_{ij}}\varphi_l|_{\Gamma_{ij}} dS \\ &= \left(\sum_{k,m}^{n_p} G'_{jkm}u_m\varphi_l\right)\Big|_{\Gamma_{i\ell b}} + \left(\sum_{k,m}^{n_p} G'_{jkm}u_m\varphi_l\right)\Big|_{\Gamma_{b\ell i}} \end{aligned} \tag{3.8}$$

depend on a local stencil of elements that is two elements thick, precisely as one would expect. The notation in (3.8) $\Gamma_{i\ell b}$ is used to denote this multilayer dependence; that is, the evaluation $\Gamma_{i\ell b}$ indicates that G' depends on a two-element thick local stencil. The evaluation for element Ω_i depends on its neighbor Ω_ℓ and the neighbor of its neighbors Ω_b. Finally, as a consequence, we can rewrite the fully factored system

$$\begin{aligned} \frac{d}{dt}u^i_{jl} =& \frac{2l+1}{h}\Bigg\{ \int_{\Omega_{e_i}} \varphi_l (J_u \mathcal{L}_{\mathscr{R}j}) u_j^h \, dx + \left(\sum_{k,m}^{n_p} F'_{jkm}u_m\varphi_l\right)\Big|_{\Gamma_{i\ell}} + \left(\sum_{k,m}^{n_p} F'_{jkm}u_m\varphi_l\right)\Big|_{\Gamma_{\ell i}} \\ &+ \left(\sum_{k,m}^{n_p} G'_{jkm}u_m\varphi_l\right)\Big|_{\Gamma_{i\ell b}} + \left(\sum_{k,m}^{n_p} G'_{jkm}u_m\varphi_l\right)\Big|_{\Gamma_{b\ell i}} \\ &- \int_{\Omega_{e_i}} (J_u f_j) u_j^h \partial_x\varphi_l \, dx - \int_{\Omega_{e_i}} \sum_{k,m}^{n_p} [J_{\nabla u} g_j]_{km}\sigma_{jk}\varphi_k \partial_x\varphi_l \, dx \Bigg\}. \end{aligned} \tag{3.9}$$

3.2 Nonlinear Stability Analysis

Now, having rewritten the nonlinear system in the above form is enough to reformulate the system using a relatively straightforward von Neumann analysis. Namely, after summing over nodes l, and suppressing the element index i and the component index j on u, then using the SSP scheme from

Section 2.3 and the notation of (1.1), the first stage can be written for the left side of (3.9):

$$\begin{aligned}\boldsymbol{u}^{(0)}|_{\Omega_{e_i}} =&\boldsymbol{u}^n|_{\Omega_{e_i}},\\ \boldsymbol{u}^{(1)}|_{\Omega_{e_i}} =&\alpha_{10}\boldsymbol{u}^{(0)}|_{\Omega_{e_i}} + \Delta t\beta_{10}\mathcal{L}_0\left(\boldsymbol{u}^{(0)}|_{\Omega_{e_i}}, \mathcal{L}\right).\end{aligned} \tag{3.10}$$

This means we can decompose the right hand side operator in the following way,

$$\begin{aligned}\boldsymbol{u}^{(0)}|_{\Omega_{e_i}} =&\boldsymbol{u}^n|_{\Omega_{e_i}},\\ \boldsymbol{u}^{(1)}|_{\Omega_{e_i}} =&A(\tilde{\mathcal{L}}, \mathcal{L}_{\mathscr{R}})\boldsymbol{u}^{(0)}|_{\Omega_{e_i}} + B(\tilde{\mathcal{L}})\boldsymbol{u}^{(0)}|_{\Gamma_{ij}} + C(\tilde{\mathcal{L}})\boldsymbol{u}^{(0)}|_{\Gamma_{ji}}\\ &+ D(\tilde{\mathcal{L}})\boldsymbol{u}^{(0)}|_{\Omega_{e_j}} + E(\tilde{\mathcal{L}})\boldsymbol{u}^{(0)}|_{\Gamma_{jk}} + F(\tilde{\mathcal{L}})\boldsymbol{u}^{(0)}|_{\Gamma_{kj}},\end{aligned} \tag{3.11}$$

where the matrices A, B, C, D, E, and F can be explicitly formed relative to a choice of $\tilde{\mathcal{L}}(\mathcal{L}_{\mathscr{D}}, \mathcal{L}_{\mathscr{C}})$. Note as well that the base element here is denoted with index i, its first neighbor by index j, and the neighbor of its first neighbor by index k.

For this first stage, we proceed by considering the first Fourier component of the now factored solution from (3.11) of every element j, $\boldsymbol{u}_j^{(1)} = \tilde{\boldsymbol{u}}_j e^{i\vartheta_j}$, where $\tilde{\boldsymbol{u}}_j$ is a vector of length $(n_p + 1)$ in every component, or a matrix of size $(n_p + 1) \times N$ over the system. Note that i denotes the imaginary unit, $i^2 = -1$, and here we take $\vartheta_j = j\xi\Delta x_j$, given ξ the wavenumber. By Δx_j we mean the characteristic cell metric $h_j = \Delta x_j$ for element j. The von Neumann analysis now follows by simply expanding into Fourier modes. That is, the domain of dependence of the differential operators are determined using a straightforward application of the Fourier shift property. The Fourier expansion (and shift) is performed relative to cell ownership as characterized by lengthscale h_j, where all spatial dependencies in the coefficient tensors that are smaller than this lengthscale (i.e. for $\Delta x < h_j$) are assumed to effectively decouple relative to the discretized representation. For more details on As such, the first stage is rewritten over each element j (after including all neighboring element dependencies in (3.11)) as:

$$\boldsymbol{u}_j^{(1)} = \Big\{ \overbrace{A_j + B_j}^{\tilde{A}_j} + \overbrace{[C_j^L + D_j^L + E_j^L]}^{\tilde{B}_j} e^{-i\vartheta_j} + \overbrace{[C_j^R + D_j^R + E_j^R]}^{\tilde{C}_j} e^{i\vartheta_j} + F_j^L e^{-2i\vartheta_j} + F_j^R e^{2i\vartheta_j} \Big\} \boldsymbol{u}_j^{(0)}.$$

Here we have used the exhaustive notation C^L and C^R, for example, to denote left and right hand neighbors in one dimension, respectively, and where $\tilde{A}_j$, $\tilde{B}_j, \tilde{C}_j, F_j^L$ and F_j^R are tensors due to the linearizations chosen in (3.2) of size $(n_p + 1) \times (n_p + 1) \times N \times N$.

From here it easily follows that the prefactor for an arbitrary stage RK method becomes the following tensor as factored in each component:

$$G_j = \tilde{A}_j + \tilde{B}_j e^{-i\vartheta_j} + \tilde{C}_j e^{i\vartheta_j} + F_j^L e^{-2i\vartheta_j} + F_j^R e^{2i\vartheta_j}, \tag{3.12}$$

such that we can write the compact form at timestep t^{n+1}:

$$\boldsymbol{u}_j^{n+1} = G_j^\star \boldsymbol{u}_j^n. \tag{3.13}$$

The matrix $G_j^\star$ in (3.13) is now simply a polynomial in G_j as determined by the RK scheme. For example, the RKSSP$(2, 2)$ scheme can now be written:

$$\boldsymbol{u}_j^{n+1} = \underbrace{[\tfrac{1}{2} + \tfrac{1}{2}(G_j)^2]}_{G_j^\star} \boldsymbol{u}_j^n, \tag{3.14}$$

where details of formalizing $G^\star$, and and a simple example using Burger's equations are provided in Appendix 8.1.

Note that it is further important here to understand the structure of the G and $G^\star$ tensors. As discussed above, these tensors are of size $(n_p+1)\times(n_p+1)\times N\times N$, meaning that in each component of the vector solution $\boldsymbol{u}=(u_1,\ldots,u_N)^T$, these correspond to $(n_p+1)\times(n_p+1)\times N$ tensors. For the sake of our spectral analysis below in Section 3.3, we view these tensors of size $(n_p+1)\times(n_p+1)\times N$ in each component, as N matrices of size $(n_p+1)\times(n_p+1)$.

3.3 Discrete Nonlinear Stability Condition

From the above discussion, it is clear that considering a single component $l\leq N$ of (3.13) at timestep $n+1$ can be understood to satisfy the form:

$$\boldsymbol{u}_l^{n+1}=\sum_{j=1}^{N}G_{jl}^{\star}(t^n)\boldsymbol{u}_l^n. \tag{3.15}$$

Now let $G_{jl}^{\star}=dtG_{jl}^{\natural}+\mathbb{1}$, then by definition:

$$\sum_{j=1}^{N}G_{jl}^{\star}(t^n)\boldsymbol{u}_l^n=\left(\mathbb{1}+\sum_{j=1}^{N}dtG_{jl}^{\natural}(t^n)\right)\boldsymbol{u}_l^n. \tag{3.16}$$

Notice that the right hand side of (3.16) is just a first order expansion of the matrix exponential, such that:

$$e^{\sum_{j=1}^{N}dtG_{jl}^{\natural}}\boldsymbol{u}_l^n=\left(\mathbb{1}+\sum_{j=1}^{N}dtG_{jl}^{\natural}(t^n)\right)\boldsymbol{u}_l^n+\mathcal{O}(dt^2).$$

As a consequence, the classical Trotter formulas [see eq. 6 in [47]] can be applied for each matrix, such that the error is effectively determined from the residual of the commutators $[dtG_{jl}^{\natural},dtG_{il}^{\natural}]$ for $j\neq i$ in each. That is,

$$e^{\sum_{j=1}^{N}dtG_{jl}^{\natural}}\boldsymbol{u}_l^n=\prod_{j=1}^{N}e^{dtG_{jl}^{\natural}}\boldsymbol{u}_l^n+\mathcal{O}(dt^2). \tag{3.17}$$

Again using a first order expansion of the matrix exponential on the right hand side of (3.17), followed by a substitution of the definition of $G_{jl}^{\natural}$, we arrive with,

$$\begin{aligned}\prod_{j=1}^{N}e^{dtG_{jl}^{\natural}}\boldsymbol{u}_l^n+\mathcal{O}(dt^2)&=\prod_{j=1}^{N}\left(\mathbb{1}+dtG_{jl}^{\natural}\right)\boldsymbol{u}_l^n+\mathcal{O}(dt^2)\\&=\prod_{j=1}^{N}G_{jl}^{\star}\boldsymbol{u}_l^n+\mathcal{O}(dt^2),\end{aligned}$$

and this yields the key observation, which is that

$$\sum_{j=1}^{N}G_{jl}^{\star}(t^n)\boldsymbol{u}_l^n=\prod_{j=1}^{N}G_{jl}^{\star}\boldsymbol{u}_l^n+\mathcal{O}(dt^2).$$

This observation is used to determine the following *discrete nonlinear stability condition*.

Definition 3.1 (Discrete nonlinear stability condition)**.** *For any system satisfying (3.15) such that to first order,*

$$\boldsymbol{u}_l^{n+1} = \prod_{j=1}^{N} G_{jl}^{\star}(t^n)\boldsymbol{u}_l^n,$$

the discrete nonlinear stability condition is $\|G_{jl}^{\star}(t^n)\| \leq 1$ *for every* l *and each* j*.*

Notice now that the operator norm simply provides for each entry that

$$\|\prod_{j=1}^{N} G_{jl}^{\star}(t^n)\| \leq \prod_{j=1}^{N} \|G_{jl}^{\star}(t^n)\|,$$

but since the product norm allows for $\|G_{jl}^{\star}(t^n)\|$ to be unbounded from both above and below, we apply instead the *discrete nonlinear stability condition.*

Now, invoking standard perturbation analysis (see e.g., [4]), by perturbing the initial state vectors $\boldsymbol{u}_l^0$ with $\boldsymbol{e}_l^0$, for $l \in \{1, \ldots, N\}$, we can denote by ε_0 the bound,

$$\|\boldsymbol{e}_l^0\| \leq \varepsilon_0, \quad l \in \{1, \ldots, N\}.$$

Defining $\boldsymbol{z}^n$ through, $\boldsymbol{z}_l^{n+1} = \prod_{j=1}^{N} G_{jl}^{\star}(t^n)\boldsymbol{z}_l^n$ with $\boldsymbol{z}_l^0 = \boldsymbol{u}_l^0 + \boldsymbol{e}_l^0$, we consider

$$\boldsymbol{e}_l^n = \boldsymbol{z}_l^n - \boldsymbol{u}_l^n, \quad n \geq 1,$$

and seek a sufficient condition ensuring $\|\boldsymbol{e}_l^n\| \leq \|\boldsymbol{e}_l^0\|$. Notice also that $\boldsymbol{e}_l^{n+1} = \prod_{j=1}^{N} G_{jl}^{\star}(t^n)\boldsymbol{e}_l^n$.

Let us recall that for a $d \times d$ matrix A, the spectral norm $\|A\|$ is given by $\|A\| = \max_{k\in\{1,\ldots,d\}} \sigma_k(A)$, where $\sigma_k(A)$ are singular values of A. Recall also that, if we denote by $\lambda_k(A)$, $k = 1, \ldots, d$, the eigenvalues of A,

$$\max_{k\in\{1,\ldots,d\}} |\lambda_k(A)| \leq \|A\|. \tag{3.18}$$

Theorem 3.2 (Nonlinear stability)**.** *Suppose the discrete nonlinear stability condition is satisfied for every time* $t^n \geq 0$*. Then, we have*

$$\|\boldsymbol{e}_i^n\| \leq \varepsilon_0, \quad i \in \{1, \ldots, N\}. \tag{3.19}$$

Proof. The result follows by induction. Let i be in $\{1, \ldots, N\}$, and consider the case of $n = 1$. We have,

$$\|\boldsymbol{e}_i^1\| = \Big\| \prod_{j=1}^{N} G_{ij}^{\star}(t^0)\boldsymbol{e}_j^0 \Big\| \leq \prod_{j=1}^{N} \|G_{ij}^{\star}(t^0)\| \|\boldsymbol{e}_j^0\| \leq \Big\{ \prod_{j=1}^{N} \|G_{ij}^{\star}(t^0)\| \Big\} \varepsilon_0 \leq \varepsilon_0.$$

For the inductive case, assuming (3.19) holds for n, it easily follows that,

$$\|\boldsymbol{e}_i^{n+1}\| = \Big\| \prod_{j=1}^{N} G_{ij}^{\star}(t^n)\boldsymbol{e}_j^n \Big\| \leq \prod_{j=1}^{N} \|G_{ij}^{\star}(t^n)\| \|\boldsymbol{e}_j^n\| \leq \Big\{ \prod_{j=1}^{N} \|G_{ij}^{\star}(t^n)\| \Big\} \varepsilon_0 \leq \varepsilon_0. \qquad \square$$

Recall that $\lambda_k(G_{ij}^{\star}(t^n)) = P(\lambda_k(G_{ij}(t^n))$ for a polynomial function P of G. Additionally, notice that by (3.18) we have

$$\max_{k\in\{1,\ldots,N\}} |\lambda_k(G_{ij}^{\star}(t^n))| \leq \|G_{ij}^{\star}(t^n)\|.$$

so that $\max_{k\in\{1,\ldots,N\}} |\lambda_k(G_{ij}^{\star}(t^n))| \leq 1$ (for all $i, j \in \{1, \ldots, N\}$ and $n \geq 0$) is a necessary condition for (3.19). Note also that this condition on the magnitude of the eigenvalues is not a sufficient condition for the temporal stabilization in this context. This can be contrasted with linear advection for example [17, 19], where here we require the stronger *discrete nonlinear stability condition* instead.

4 An Atmospheric Model problem

As an example problem we consider the barotropic compressible multicomponent reactive Navier-Stokes equations [9, 26, 28, 35] applied to a problem arising in atmospheric chemistry.

4.1 Multicomponent Reactive Navier-Stokes

Considering a barotropic pressure law $p(\rho_i)$, and a pressure-dependent constitutive relation for the viscosity $\eta(p)$, we are interested in solving the following system of equations

$$\partial_t(\rho v) + \partial_x(\rho v^2) + \partial_x p(\rho) - \partial_x(\eta(p)\partial_x v) = 0, \tag{4.1}$$

$$\partial_t \rho_i + \partial_x(\rho_i v) = \mathscr{A}_i(\mathring{n}), \tag{4.2}$$

where $\mathscr{A} = \mathcal{L}_{\mathscr{R}}$ is the law of mass action calculated relative to the forward k_f and backward k_b reaction rates (in units of $\mathrm{m}^3\mathrm{molecule}^{-1}\mathrm{s}^{-1}$). The mass action law in general satisfies the form

$$\mathscr{A}_i(\mathring{n}) = m_i \sum_{r\in\mathfrak{R}} (\nu_{ir}^b - \nu_{ir}^f) \left(k_{fr} \prod_{j=1}^{n} n_j^{\nu_{jr}^f} - k_{br} \prod_{j=1}^{n} n_j^{\nu_{jr}^b} \right). \tag{4.3}$$

The molar concentration n_i of the ith chemical constituent in (4.3), up to a scaling by Avogadro's constant N_A, is just the number density $n_i = N_A \mathfrak{n}_i$. We use this convention since, as we will see below, the reaction rates are often formulated in molar units. The species are given by $\rho_i = \rho\mu_i = m_i n_i$ where μ_i is the mass fraction of the ith species, and m_i is the molar mass of the ith species. The total density is recovered additively $\rho = \sum_i \rho_i$, while the barotropic pressure law can be written as a sum of partial pressures p_i, such that $p = \sum_i p_i = \sum_i \rho_i^{\gamma_i}$, for γ_i the adiabatic index of each constituent. The viscosity will be taken to satisfy the scalar constitutive law, $\eta = Cp^{-\alpha} \sum_i \rho_i \partial_{\rho_i} p$, for α a positive constant between zero and one, and $C \in R^+$.

The forward and backward stoichiometric coefficients of elementary reaction $r \in \mathbb{N}$ are given by $\nu_{ir}^f \in \mathbb{N}$ and $\nu_{ir}^b \in \mathbb{N}$, while $k_{fr}, k_{br} \in \mathbb{R}$ are the respective forward and backward reaction rates of reaction r. These terms serve to define the mass action $\mathscr{A}_i = \mathscr{A}_i(\mathring{n})$ of the reaction. Moreover, we denote the indexing sets $\mathscr{R}^r$ and $\mathscr{P}^r$ as the reactant and product wells $\mathscr{R}^r \subset \mathbb{N}$ and $\mathscr{P}^r \subset \mathbb{N}$ for reaction r. Then for a reaction indexed by $r \in \mathfrak{R}$, occurring in a chemical reactor $\mathfrak{R} \subset \mathbb{N}$, comprised of n distinct chemical species $\mathfrak{M}_i$ the following system of chemical equations are satisfied,

$$\sum_{j\in\mathscr{R}^r} \nu_{jr}^f \mathfrak{M}_j \underset{k_{br}}{\overset{k_{fr}}{\rightleftharpoons}} \sum_{k\in\mathscr{P}^r} \nu_{kr}^b \mathfrak{M}_k, \quad \forall r \in \mathfrak{R}. \tag{4.4}$$

Equation (4.1)-(4.2) obey a standard mass conservation principle as the elementary reactions are balanced, the conservation of atoms in the system is an immediate consequence of (4.4). Let $\mathfrak{a}_{il}$ be the lth atom of the ith species $\mathfrak{M}_i$, where $l \in \mathfrak{A}^r$ is the indexing set $\mathfrak{A}^r = \{1, 2, \ldots, n_{atoms,r}\}$ of distinct atoms present in each reaction $r \in \mathfrak{R}$. Then the total atom conservation is satisfied for every atom in every reaction

$$\sum_{i\in\mathscr{R}^r} \mathfrak{a}_{il}\nu_{ir}^f = \sum_{i\in\mathscr{P}^r} \mathfrak{a}_{il}\nu_{ir}^b \quad r \in \mathfrak{R},\ l \in \mathfrak{A}^r. \tag{4.5}$$

Since the total number of atoms is conserved, so is the total mass in each reaction,

$$\sum_{i\in\mathscr{R}^r} m_i\nu_{ir}^f = \sum_{i\in\mathscr{P}^r} m_i\nu_{ir}^b \quad \forall r \in \mathfrak{R}. \tag{4.6}$$

It then immediately follows that integration yields the following bulk conservation principle satisfied globally:

$$\frac{d}{dt}\sum_{i=1}^{n}\int_\Omega \rho_i\, dx = 0. \tag{4.7}$$

We solve the system (4.1) and (4.2) for the $n = 9$ fluid of atmospheric gas phase organic halogen reactions [5, viz. reactions 88 and 89]:

$$\begin{aligned} \mathrm{Cl}^\bullet + \mathrm{HC(O)Cl} &\xrightarrow{k_1} \mathrm{HCl} + \mathrm{ClCO}^\bullet \\ \mathrm{Cl}^\bullet + \mathrm{CH_3OCl} \xrightarrow{k_2} \mathrm{Cl_2} + \mathrm{CH_3O}^\bullet &\xrightarrow{k_3} \mathrm{HCl} + \mathrm{CH_2OCl}^\bullet \end{aligned} \tag{4.8}$$

Here high energy chlorine radicals (an important species in ozone depletion) develop due to photodissociation from sufficient actinic flux of UV radiance, and subsequently react with formyl chloride HC(O)Cl) and methyl hypochlorite (CH_3OCl) to produce chlorocarbonyl ($ClCO^\bullet$) radicals, HCl, chloride gas, and a methoxy ($CH_3O^\bullet$) radical. The final product of this reaction is the $CH_2OCl^\bullet$ radical, which is an important intermediate in the atmospheric oxidation of methyl chloride (CH_3Cl), or chloromethane, the most prevalent halocarbon in the atmosphere, with a global average tropospheric abundance of 600 pptv [48]. It should be noted that as a subsystem (4.8) can be written as a collection of ordinary differential equations, leading to chaotic dynamics in the reactive subsystem [27].

4.2 The State Vector Form

So let us take a look at what this means in the above notation. The operator $\mathcal{L}$ can now be written out explicitly relative to ten-vector, $\boldsymbol{u} = (\rho v, \rho_1, \ldots, \rho_9)^\top$, where

$$(\rho_1, \ldots, \rho_9)^\top = (\mathrm{Cl}^\bullet, \mathrm{HCl}, \mathrm{Cl_2}, \mathrm{CH_3OCl}, \mathrm{CH_2OCl}^\bullet, \mathrm{CH_3O}^\bullet, \mathrm{HC(O)Cl}^\bullet, \mathrm{ClCO}^\bullet, \mathrm{bath})^\top.$$

The convective fluxes are given explicitly as $\boldsymbol{f} = (\rho v^2, \rho_1 v, \ldots, \rho_9 v)^\top$, the diffusive fluxes as

$$\boldsymbol{g} = (\eta\partial_x v, 0, \ldots, 0)^\top,$$

and the mass action by

$$\mathscr{A}_i(\mathring{n}) = \begin{pmatrix} 0 \\ -m_1(k_1 n_1 n_7 + k_2 n_1 n_4) \\ m_2(k_1 n_1 n_7 + k_3 n_3 n_6) \\ m_3(k_2 n_1 n_4 - k_3 n_3 n_6) \\ -m_4 k_2 n_1 n_4 \\ m_5 k_3 n_3 n_6 \\ m_6(k_2 n_1 n_4 - k_3 n_3 n_6) \\ -m_7 k_1 n_1 n_7 \\ m_8 k_1 n_1 n_7 \end{pmatrix}$$

The convective flux $\boldsymbol{f} = (\rho v^2 + p, \rho_1 v, \ldots, \rho_9 v)^\top$ has the following Jacobian matrix

$$J_{\boldsymbol{u}}\boldsymbol{f} = \begin{pmatrix} 2v & \chi_1 & \chi_2 & \ldots & \ldots & \chi_9 \\ \mu_1 & v(1-\mu_1) & -\mu_1 v & \ldots & \ldots & -\mu_1 v \\ \mu_2 & -\mu_2 v & v(1-\mu_2) & -\mu_2 v & \ldots & \vdots \\ \vdots & \vdots & \ddots & \ddots & \ddots & \vdots \\ \vdots & \vdots & \ddots & \ddots & \ddots & \vdots \\ \mu_9 & -\mu_9 v & \ldots & \ldots & \ldots & v(1-\mu_9) \end{pmatrix}.$$

where $\chi_i = \partial_{\rho_i} p_i - v^2$. Similarly the diffusive flux can be written relative to the following matrix:

$$J_{\nabla \boldsymbol{u}}\boldsymbol{g} = \eta \begin{pmatrix} \rho^{-1} & -\rho^{-1}u & \ldots & -\rho^{-1}u \\ \mathbf{0} & \mathbf{0} & \ldots & \mathbf{0} \end{pmatrix},$$

with the zero-vector $\mathbf{0}$ of length n. Finally, the Jacobian matrix of the operator $\mathcal{L}_{\mathscr{R}i}(u_h(x,t),t)$ with respect to $(\rho_1, \ldots, \rho_9)^\top$ is written:

$$J_{\boldsymbol{u}}\mathscr{A}(\mathring{n}) = \begin{pmatrix} 0 & 0 & 0 & 0 & 0 & 0 & 0 & 0 & 0 \\ -(\frac{k_1\rho_7}{m_7} + \frac{k_2\rho_4}{m_4}) & 0 & 0 & -\frac{k_1\rho_1}{m_4} & 0 & 0 & -\frac{k_1\rho_7}{m_7} & 0 & 0 \\ \frac{m_2k_1\rho_7}{m_1m_7} & 0 & \frac{m_2k_3\rho_6}{m_3m_6} & 0 & 0 & \frac{m_2k_3\rho_3}{m_3m_6} & \frac{m_2k_1\rho_1}{m_1m_7} & 0 & 0 \\ \frac{m_3k_2\rho_4}{m_1m_4} & 0 & -\frac{k_3\rho_6}{m_6} & \frac{m_3k_2\rho_1}{m_1m_4} & 0 & -\frac{k_3\rho_3}{m_6} & 0 & 0 & 0 \\ -\frac{k_2\rho_5}{m_1} & 0 & 0 & -\frac{k_2\rho_1}{m_1} & 0 & 0 & 0 & 0 & 0 \\ 0 & 0 & \frac{m_5k_3\rho_6}{m_3m_6} & 0 & 0 & \frac{m_5k_3\rho_3}{m_3m_6} & 0 & 0 & 0 \\ \frac{m_6k_2\rho_4}{m_1m_4} & 0 & -\frac{k_3\rho_6}{m_3} & \frac{m_6k_2\rho_1}{m_1m_4} & 0 & -\frac{k_3\rho_3}{m_6} & 0 & 0 & 0 \\ -\frac{k_1\rho_7}{m_1} & 0 & 0 & 0 & 0 & 0 & -\frac{k_1\rho_1}{m_1} & 0 & 0 \\ 0 & 0 & 0 & 0 & 0 & 0 & 0 & 0 & 0 \\ 0 & 0 & 0 & 0 & 0 & 0 & 0 & 0 & 0 \end{pmatrix}.$$

5 Numerical Results and Experiments

Here we present basic numerical behaviors of the system 1.2 given the different spatial and temporal discretizations described in Section 2. First the basic physical regimes governing the nonlinear convection-diffusion-reaction system from Section 4 are demonstrated and explained. Next a number of stability results are presented, with an explanation of how these results relate to both the physical systems, as well as the nonlinear stability results from Section 3.

5.1 Basic Physics of the Coupled System

The various relevant physical regimes of the system can be evoked by rewriting (4.1)-(4.2) as the following rescaled initial-boundary problem:

$$\partial_t(\rho v) + \partial_x(\rho v^2) + \partial_x p(\rho) - \partial_x(\eta(p)\partial_x v) = 0, \tag{5.1}$$

$$\partial_t \rho_i + \partial_x(\rho_i v) = \mathscr{A}_i(\mathring{n}), \tag{5.2}$$

$$\rho_i|_{t=0} = \tilde{\kappa}_i \rho_{0,i}, \quad \rho_{|t=0} = \kappa_1 \rho_0, \quad v_{|t=0} = \kappa_2 v_0, \tag{5.3}$$

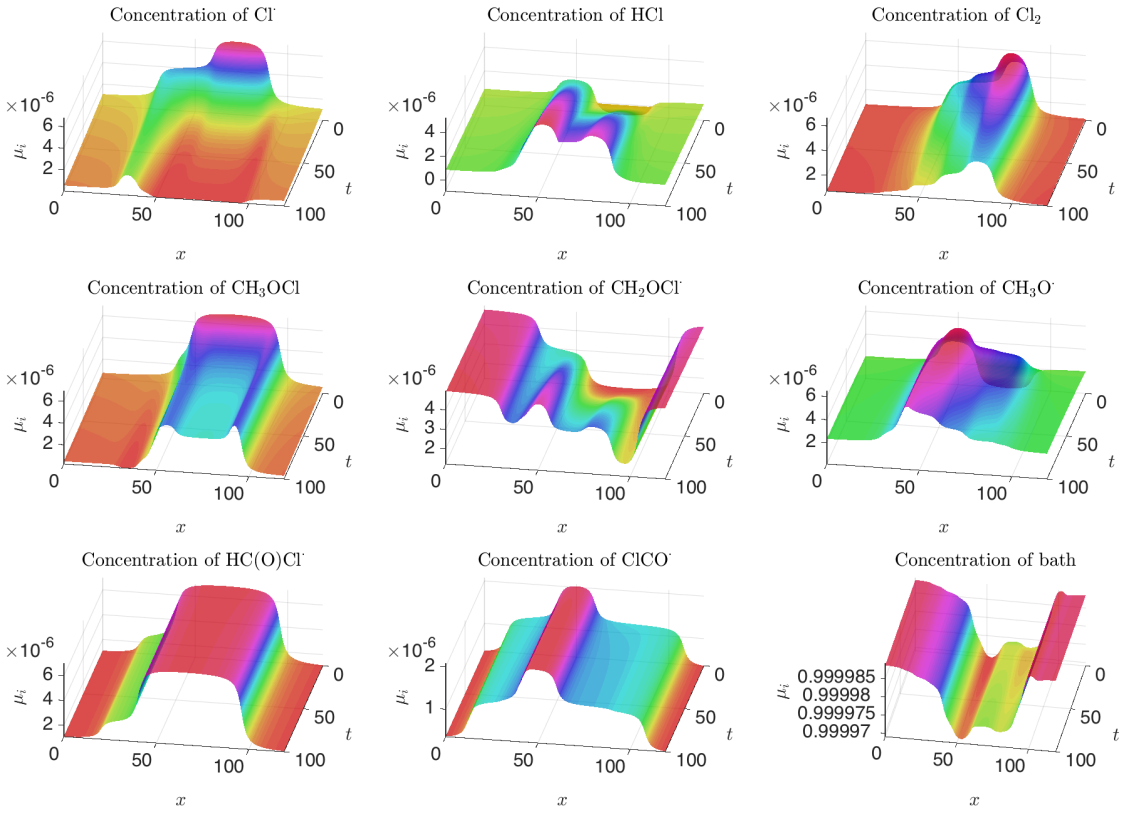

Figure 2: Here we show a reaction regnant regime, with $\alpha = 0.7$, $\kappa_3 = 10^{-4}$, the $\tilde{\kappa}_i = 0.1$, $\kappa_1 = 1$, $\kappa_2 = 10^{-4}$. The mesh includes 40 elements, $dt = .26$, and $h = 1.35$.

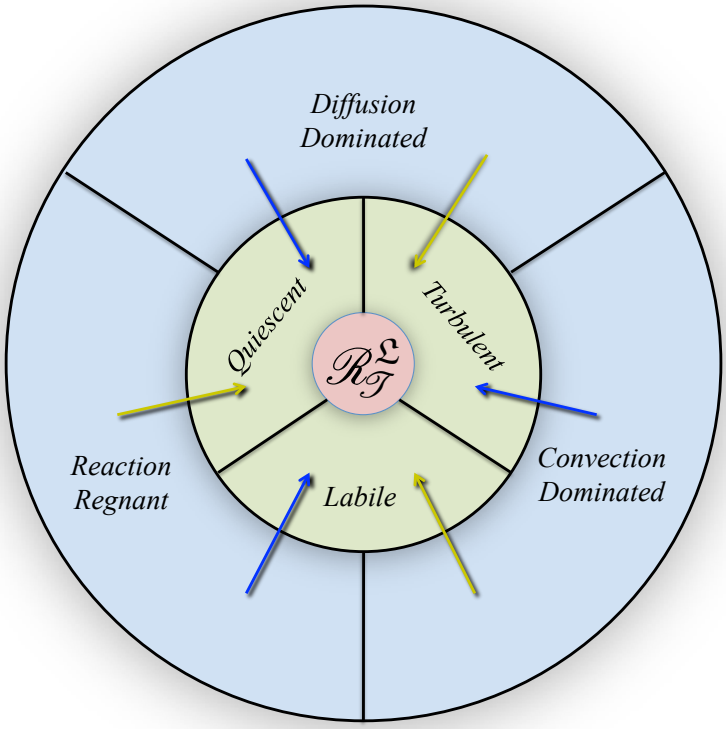

Figure 3: The physical flow regimes accessible to the coupled system (4.1)-(4.2).

assuming periodic boundary data, and the consistency condition $\rho\kappa_1 = \sum_i \rho_{0,i}\tilde{\kappa}_i$. The initial state can be seen from the fluxes in Section 4 to effectively scale the relative dynamic transport in the subsystems (as discussed in detail below). We also use a rescaled viscosity $\eta = \kappa_3 p^{-\alpha} \sum_i \rho_i \partial_{\rho_i} p$ for the same purpose.

In this system we characterize three standard regimes: convection dominated, diffusion dominated, and reaction regnant. These regimes can be formally derived using kinetic theory (see Fig. 3, and for background see [27]). The three regimes can be qualitatively understood using by way of the following characterizations: 1) convection dominated flows are those driven by convective fluxes having a qualitatively "hyperbolic flavor,", 2) diffusion dominated flows are those driven by diffusive effects (e.g. viscosity) having a qualitatively "parabolic flavor," and 3) reaction regnant flows are those driven by an n-coupled system of first order autonomous nonlinear ordinary differential equations (or nFANODEs, see [27] for more details).

These three regimes elicit the possibility of four additional mixed-state regimes that encompass large classes of frequently encountered flows in nonlinear application models. A graphical representation of these flow relations is provided in Fig. 3. More clearly, systems where the convective modes of the system have similar scalings to the diffusive modes of the system, but do so without appreciable reactions, are characterized here as turbulent flows $\mathscr{T}$. For example, single component high Reynold's number flows with large eddy viscosity are turbulent flows. When diffusive modes

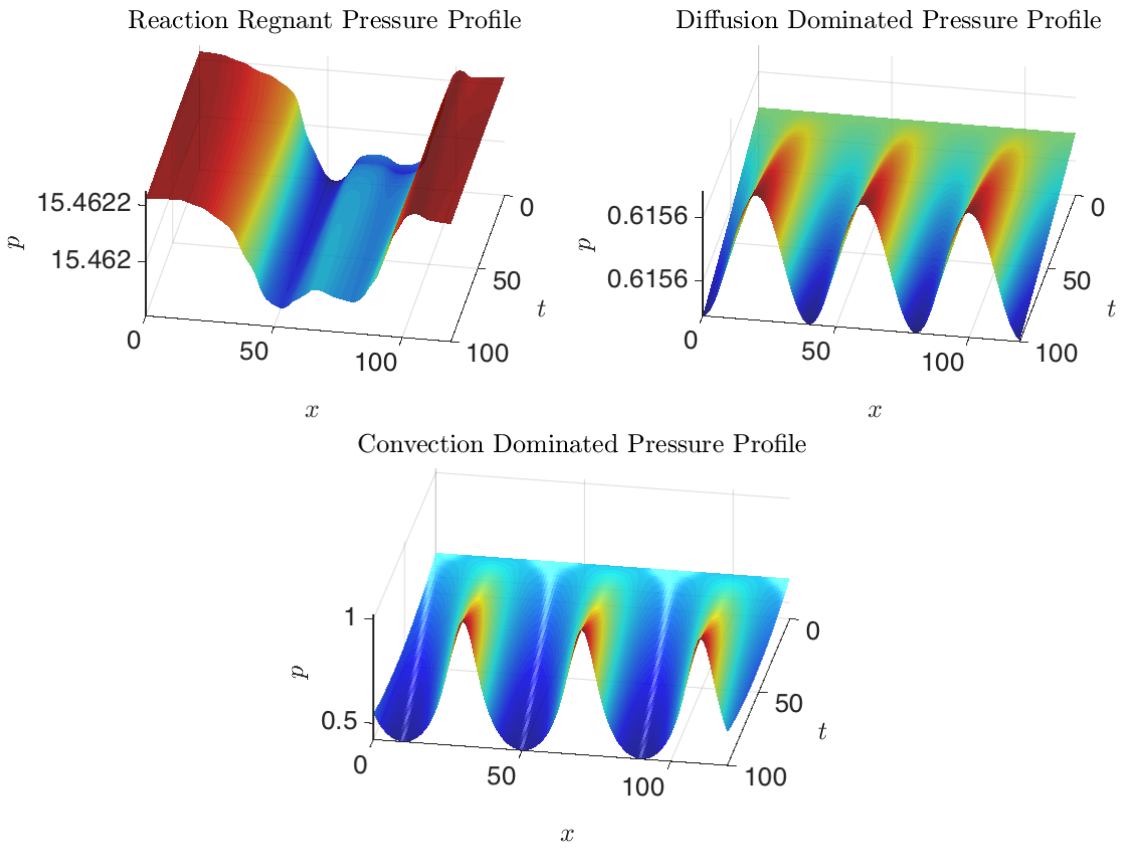

Figure 4: The pressure $p = \sum_i \rho_i^{\gamma_i}$ profiles for a reaction regnant solution (top left), a diffusion/viscosity dominated solution (top right), and a convection dominated solution (bottom center).

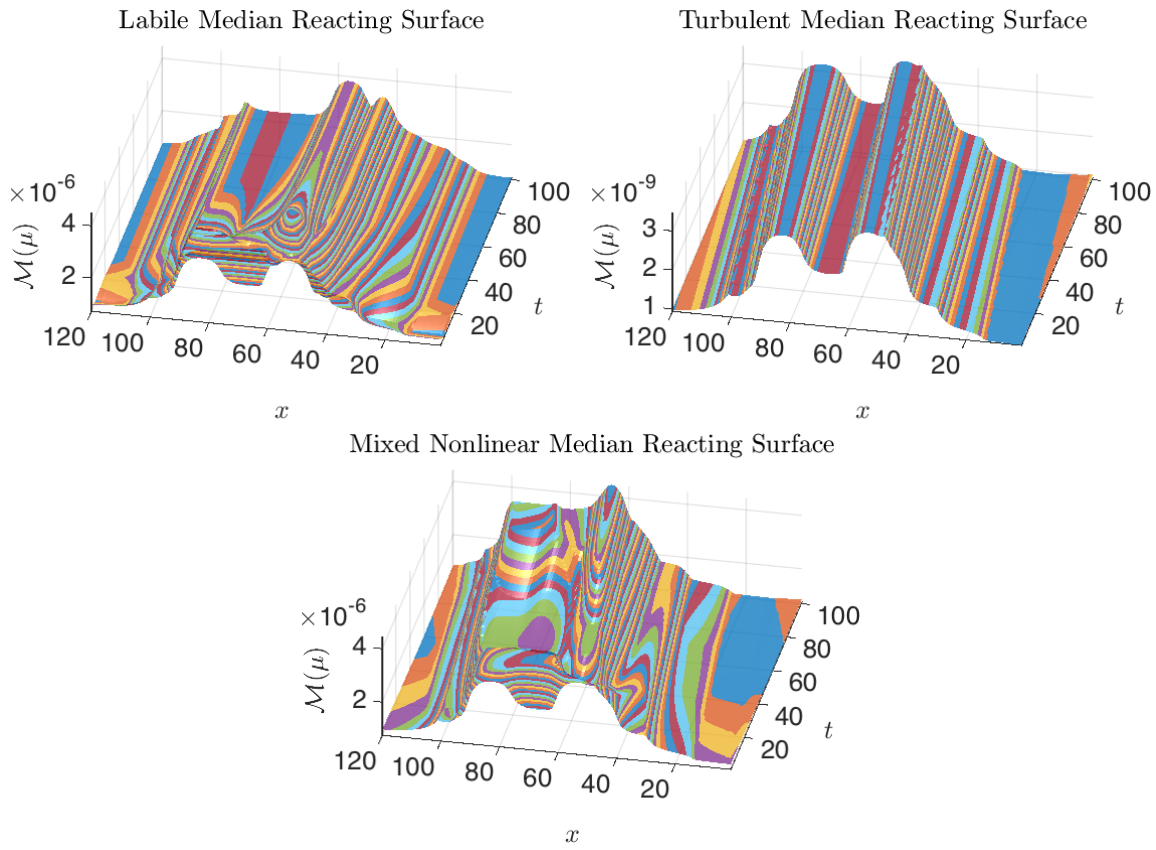

Figure 5: The median reacting surface $\mathcal{M}(\mu)$ for a labile solution (top left), a turbulent solution (top right), and a $\mathscr{R}^{\mathfrak{L}}_{\mathscr{T}}$ solution (bottom center).

have similar growth characteristics to reactive modes in the absence of appreciable convection (or mixing), one obtains a reactive quiescent flow $\mathscr{R}$, as arising in laboratory experiments in non-mixed (or quiescent) states (see [27]). When the the reactive modes evolve on scales commensurable to convective scales, where diffusive modes become negligible, the system is characterized by rapidly changing transitory states, and is characterized as labile $\mathfrak{L}$, as seen in explosive detonations, chain reactions, and flow cascades, etc. Finally, when all three regimes are competing, e.g. when the convective, diffusive, and reactive modes all occur on similar scalings, the flow is characterized as a reacting turbulent labile flow $\mathscr{R}^{\mathfrak{L}}_{\mathscr{T}}$, such as occur (often locally) in high energy reactor systems.

The regimes discussed above are inherent to the nonlinear system (4.1)-(4.2), and indeed to any nonlinear convection-diffusive-reactive system (1.1). An easy way to force the system between the different regimes, in order to probe sensitivities and responses within the coupled system, is to simply scale the κ_i's and $\tilde{\kappa}_i$ in (5.1)-(5.3). On a basic level, these rescalings effectively weight the flux jacobians from Section 4, thus amplifying the basic character of the solution relative to a particular regime. For example, if we increase $\tilde{\kappa}_i$, then the ρ_i are upscaled as a consequence, implying the entries in the reactive Jacobian matrix $J_{\rho_i}\mathscr{A}(\mathring{n})$ get upscaled and the reactive character of the flow is (at least initially) enhanced. Similarly we can increase the convective nature of the flow my increasing κ_1 or κ_2, though we have to be careful, since increasing the $\tilde{\kappa}_i$ also enhances the

nonlinearities present in the pressure-driven convection. These inter-related nonlinear responses are inherent of course to nonlinear dynamics, and come as no surprise. Finally, if we want to enhance the diffusion regime, we can simply increase the viscosity scaling using κ_3. It can be noted here that though initial conditions offer an easy way to navigate between the different regimes, it is by no means the only way to do so. We could similarly use boundary forcings, or even construct evolution states that reach perturbed equilibria, or dynamic cascades that push between different regimes. In general, even for a flow that is initially reaction regnant, the natural dynamics of the system can evolve in time to, for example, a turbulent regime; or one where the reactions have exhausted to some metastable equilibrium, and so forth.

Take as an example a reaction regnant solution. In Fig. 2 we show such a solution, where the chemical subsystem (4.8) completely dominates the dynamics of the system over 100 timesteps. This is achieved by tuning the κ and $\tilde{\kappa}$ parameters, as notated in Fig. 2. In this regime, the dynamical subsystem determined by $\mathcal{L}_{\mathscr{R}}$ completely characterizes the relevant temporal constraints. The initial species densities of the components are given as linear combinations of smooth functions, which can be seen on Fig. 2, while the initial momentum and total density are chosen as periodic sinusoidal functions. These conditions are chosen to help differentiate and visualize the influence from the reaction, the convection, and diffusion diffusion in the various regimes. Similarly, this initial data drives the solutions shown in figures 4 and 5, where aspects of the regimes above are shown on a simple example. In Fig. 4 the barotropic pressure profiles are provided over each solution regime. In this example, in the absence of appreciable convection (e.g. the reaction regnant or quiescent regimes) the pressure is driven by local perturbations in the reactive species density.

Similarly in Fig. 5, we show the median reaction surface $\mathcal{M}(\mu)$. This surface is computed over the mass fractions μ_l at each quadrature points n_q and timesteps n_t according to

$$\mathcal{M}(\mu(x_i, t_j)) = \underset{l \leq N}{\text{median}}\, \mu_l(x_i, t_j).$$

Since the bath component μ_9, for example, should completely dilute the average value over the N species (by virtue of the definition of a negligibly inert background chemical bath), the median is a more natural measure of the effective relative approximate reacting character of the multicomponent system. In Fig.5 the contour shadings (i.e. the approximate system isoclines of the surface) emphasize the relative local variation that the species densities experiences in the presence of strong reactive components (i.e. labile and $\mathscr{R}^{\mathfrak{L}}_{\mathscr{T}}$ flows), while the turbulent flow shows smooth variance driven by diffusive-convecting transport. Also note the absence of appreciable chemical repellers and attractors in the strictly turbulent regime, while when the reactive modes are more impactful, the topology of the isoclines becomes more interesting.

5.2 Stability Behavior in Nonlinear Systems

Finally let us take a look at the stability properties of the example problem posed in Section 5.1. Here we use a timestep of $dt = h/18$ for every case in the figures presented below (unless otherwise stated), primarily for the sake of comparison between the various regimes, though we do discuss how the choice of timestep affects the results in the accompanying text. Notably, reducing the timestep is always a way of achieving stability in the sense of Theorem 3.2 for this example system. The examples are chosen to highlight the differences between the RKC and RKSSP schemes, as well as the relationships between the various regimes shown in Fig. 3. Also note that we analyze the eigenspectrum by restricting to a single element in the center of the domain for each case. The

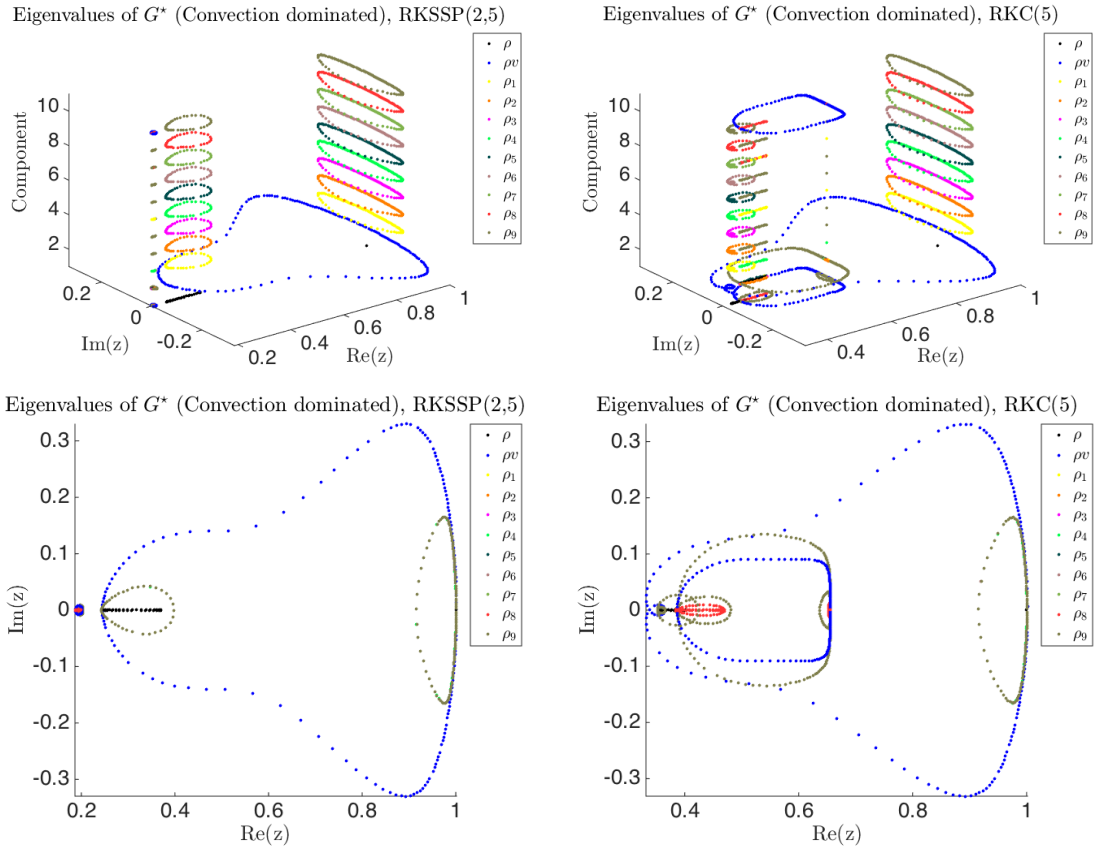

Figure 6: For a convection dominated problem we show $G^\star$, with $dt = h/18$, for the RKSSP(2,5) on the left, and RKC(5), $\epsilon = .15$ on the right.

eigenspectrum is also provided for each of these examples to highlight how different (and irregular) the nonlinear spectrum is relative to the strictly linear case (viz. [20]).

In the (nonlinear) convection dominated case we first consider the problem using the notation from Section 5.1, with $\kappa_1 = 1$, $\kappa_2 = 0.5$, $\tilde{\kappa}_i = 10^{-4}$ for $i = 1, \ldots, 8$, and $\tilde{\kappa}_9$ determined from the consistency condition. The viscosity scaling is $\kappa_3 = 10^{-4}$. In this setting the reactive modes are nearly completely suppressed, as are the diffusive modes, leaving primarily the nonlinear convective fluxes. In Fig. 6 however, even when the reactive and diffusive modes are suppressed, the presence of the nonlinearity in the convective modes is still enough, it turns out, to show remarkable differences in the eigenstructures corresponding to the RKC and the RKSSP schemes. Note from Fig. 1 that the RKC(5) regime with $\epsilon = 0.15$ is a longer and thinner stability region than the RKSSP(2,5) stability region. In Fig. 6 both regimes are stable at a timestep of $dt = h/18$, and it is also interesting, as shown in Fig. 7, that significant nested spectrum are present in both regimes, though at remarkably different scales in terms of the amplitude of eigenvalues between the RKC and RKSSP, where the RKC scheme seems to amplify the structural content of the eigenstructure in comparison to the RKSSP scheme in this case.

In the reaction regnant regime, we set $\kappa_1 = 20$, $\kappa_2 = 10^{-4}$, $\tilde{\kappa}_i = 1$ for $i = 1, \ldots, 8$ and $\tilde{\kappa}_9$ determined from the consistency condition. The viscosity scaling is again taken as $\kappa_3 = 10^{-4}$.

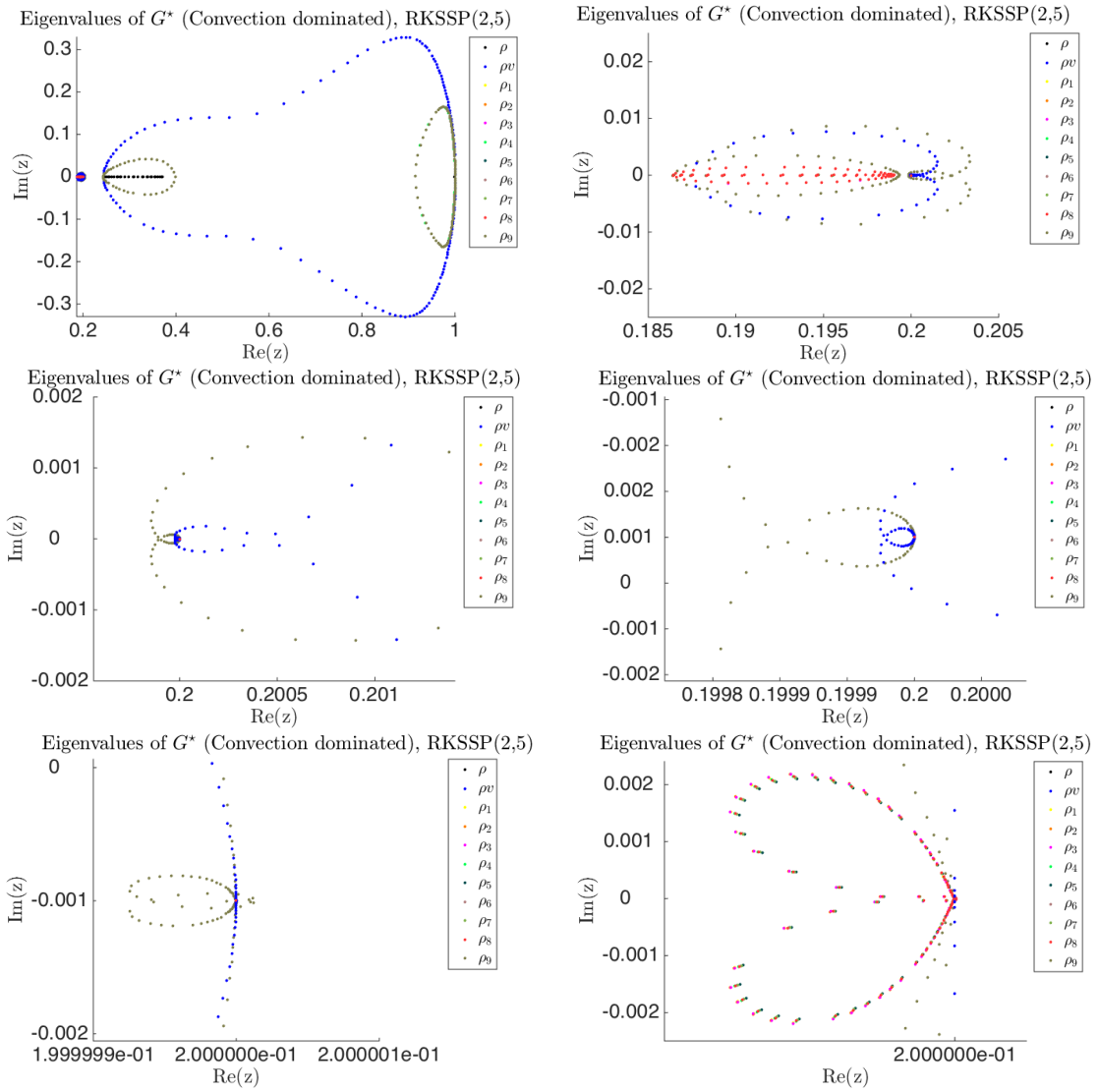

Figure 7: Here we show nested zooms of $G^\star$ the RKSSP(2,5) solution to the convection dominated regime shown in Fig. 6.

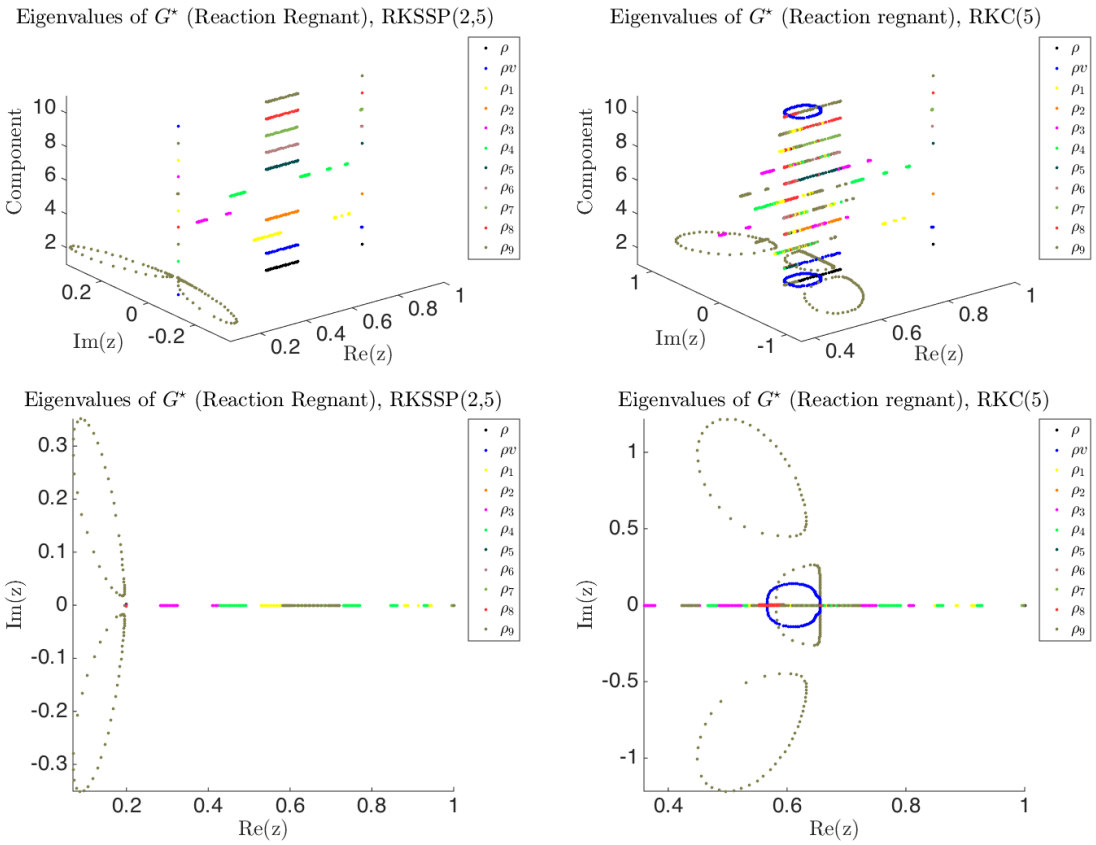

Figure 8: The reaction regnant spectrum of $G^\star$ for RKSSP(2,5) on the left, and RKC(5), $\epsilon = 0.15$ on the right.

Notice how different the spectrum is from the (nonlinear) convection dominated regime in Fig. 6 to the reaction regnant regime in Fig. 8. Perhaps the most compelling difference is how suppressed the reactive modes look to be in the RKSSP(2,5) scheme, in comparison to the RKC(5), $\epsilon = 0.15$ scheme. In fact, this is what we observe to frequently be the case between these two regimes: the RKSSP scheme seems to produce much less elaborate eigenstructures than the RKC schemes. In this case however, this is to the benefit of the stability, as the RKSSP(2,5) scheme in Fig. 8 is inside the stability region while the RKC(5) scheme is not. Nevertheless, both solutions appear robust at the given timestep when plotting out the state vector of unknowns u, highlighting the fact that even solutions that may "appear to be stable," may in fact not be evolving in a fully stable regime.

The diffusion dominated regime is set using the following: $\kappa_1 = 1$, $\kappa_2 = 10^{-4}$, $\tilde{\kappa}_i = 10^{-4}$ for $i = 1, \ldots, 8$ with $\tilde{\kappa}_9$ determined from the consistency condition, and viscosity scaling $\kappa_3 = 0.5$. Here we see dramatic differences between the RKC(5), $\epsilon = 0.15$ and RKSSP(2,5) schemes, where the RKC scheme seems to develop a substantially finer structure, as seen in Fig. 9. Not entirely surprisingly, the diffusion dominated regime shows a characteristic stiffness in both RK schemes, where even though the majority of the modes are within the stability region, small perturbations near $\mathrm{Re}(z) = 1$ send the eigenvalues into slightly unstable regions leading to both schemes being slightly unstable in the sense of theorem 3.2. Moreover, in contrast to the reaction regnant subsystem, the diffusion dominated regime seems to be much more sensitive to unstable eigenvalues, where even very slight perturbations from the stability region are immediately visible in the actual solution u. It is therefore essential to preserve stabilization in the diffusion dominated system, and in order to do so, smaller timesteps must be chosen, which is in accordance with the standard approximate CFL heuristics for linear parabolic-type subproblems.

Mixing together the relatively "pure" regimes (i.e. convection dominated, reaction regnant, and diffusion dominated from Fig. 3), one immediately see more elaborate behavior in the eigenstructure of the solution. For the labile example, we set $\kappa_1 = 20$, $\kappa_2 = 0.5$, $\tilde{\kappa}_i = 1$ for $i = 1, \ldots, 8$ and $\tilde{\kappa}_9$ determined from the consistency condition, with viscosity scaling $\kappa_3 = 10^{-3}$. In Fig. 10 it is clear that the reaction modes are also "extended" by the RKC regime, in comparison to the RKSSP regime, and moreover, in this example, as with the reaction regnant model in Fig. 8, become slightly unstable in the sense of Theorem 3.2 only in the RKC, $\epsilon = 0.15$ scheme. However, also as in Fig. 8, this instability does not lead to a visible loss of stability in the solution u. In this particular example, one can stabilize these effects easily by increasing $\epsilon = 5$, wherein the thick regions match much more closely to those in the RKSSP scheme, but some of the thin region spectrum remains. This leads to a broader, more structured spectrum that is still stable under Theorem 3.2.

In the case of turbulent driven flows, we use the settings: $\kappa_1 = 1$, $\kappa_2 = 0.5$, $\tilde{\kappa}_i = 10^{-4}$ for $i = 1, \ldots, 8$, and $\tilde{\kappa}_9$ determined from the consistency condition, with viscosity scaling $\kappa_3 = 0.35$. Here again, the differences caused by the nonlinear pressure term p, that also directly drives the viscosity $\eta(p)$, is not particularly subtle. In this case, with $dt = h/18$, both the RKSSP and RKC schemes are stable according to Theorem 3.2, though the spectra are radically different, as seen in Fig. 11.

Finally, in the fully mixed regime $\mathscr{R}^{\mathcal{L}}_{\mathcal{F}}$ from Fig. 3, we set: $\kappa_1 = 10$, $\kappa_2 = 0.5$, $\tilde{\kappa}_i = 1$ for $i = 1, \ldots, 8$, and $\tilde{\kappa}_9$ determined from the consistency condition, with viscosity scaling $\kappa_3 = 0.35$. In this case the differences between the RKSSP(2,5) and the RKC(5), $\epsilon = 0.15$ are a bit surprising. Here both schemes are unstable according to Theorem 3.2, though the RKC scheme is barely unstable just along $\mathrm{Re}(z) > 1$, while the RKSSP solution goes entirely unstable, Fig. 12. This seems to be consistent with the general observation. That is, the RKC scheme seems to show a

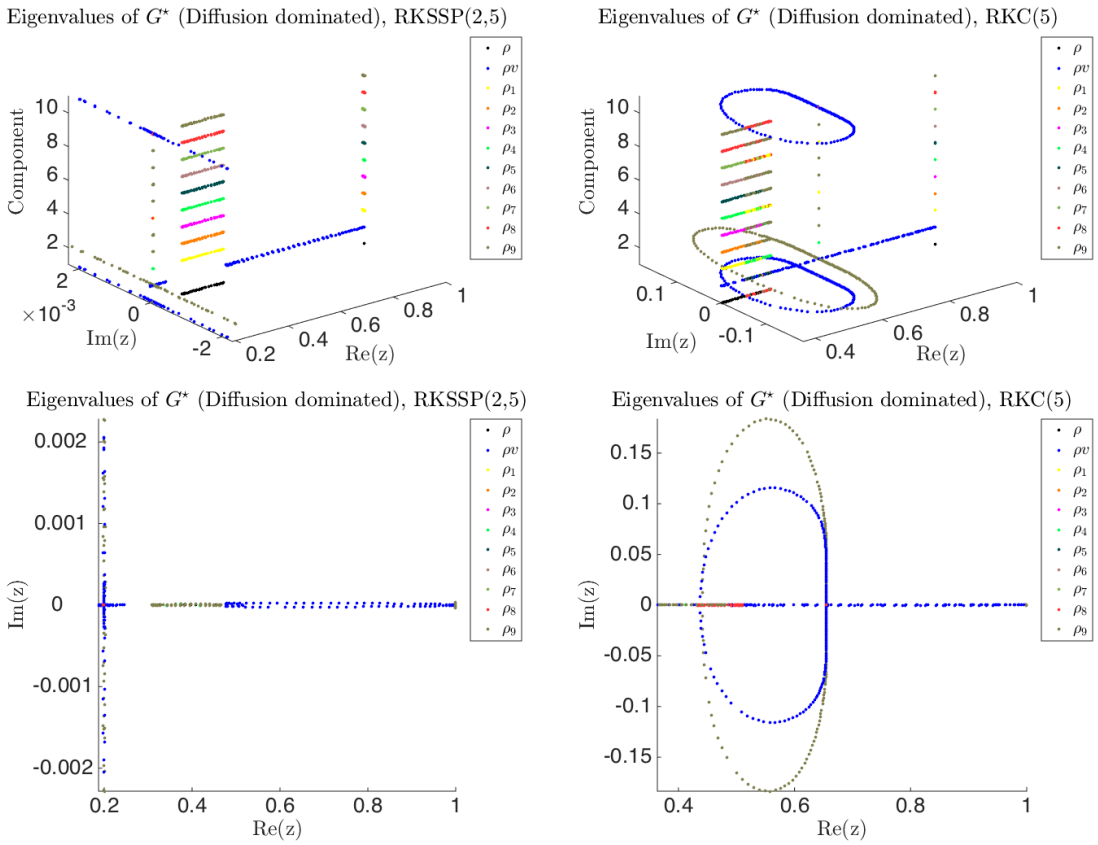

Figure 9: The diffusion dominated spectrum of $G^\star$ for the RKSSP(2,5) regime (left), and RKC(5), $\epsilon = 0.15$ (right).

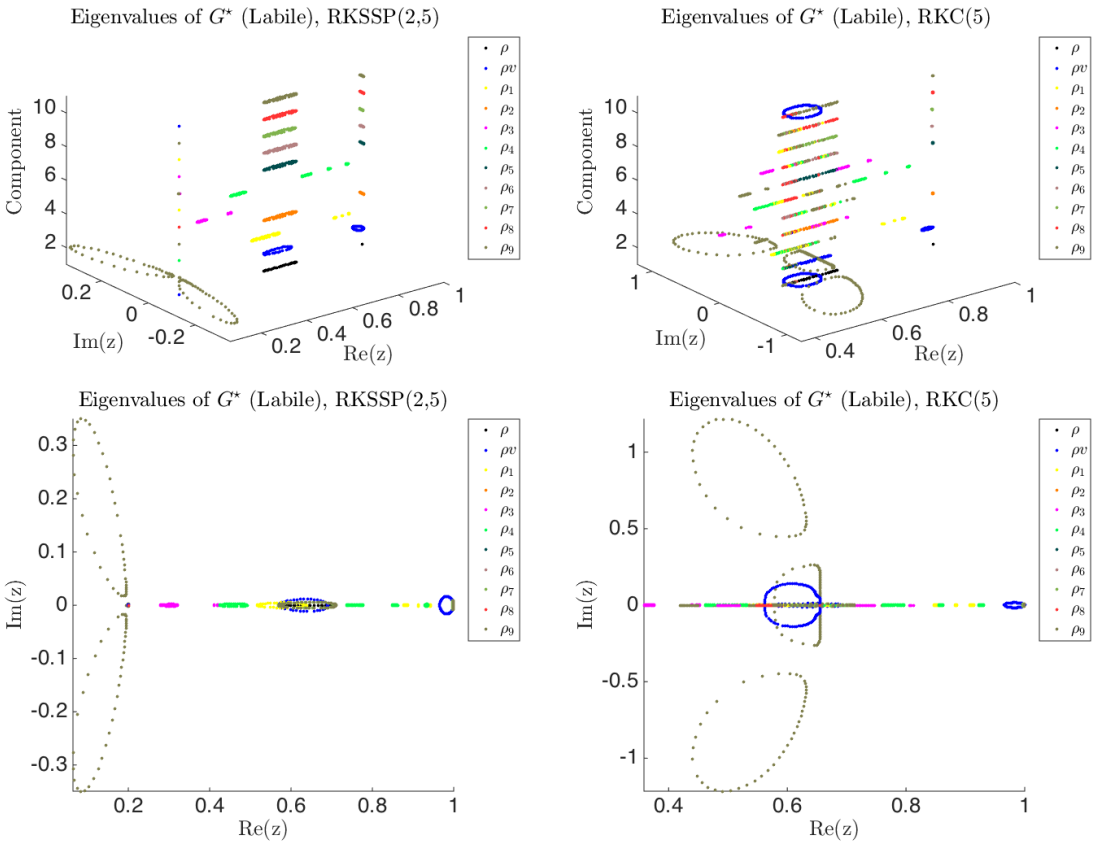

Figure 10: The labile spectrum of $G^\star$ for the RKSSP(2,5) regime (left), and RKC(5), $\epsilon = 0.15$ (right).

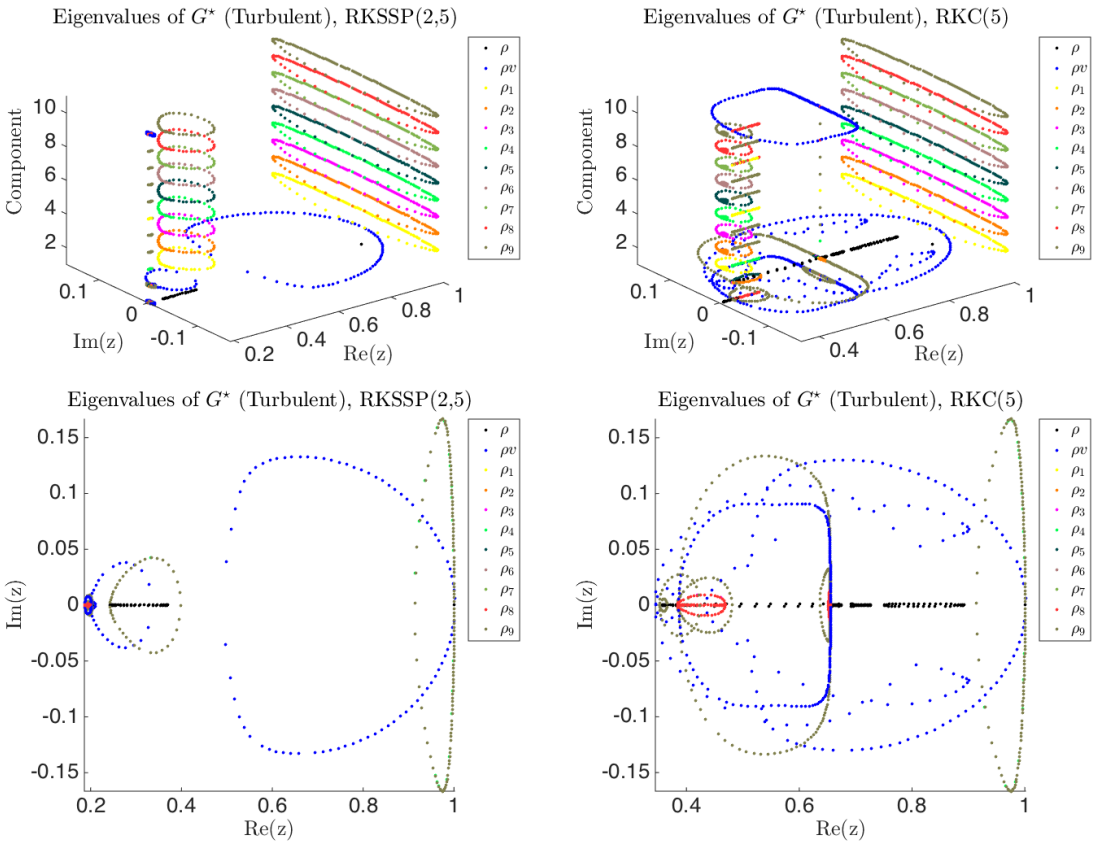

Figure 11: In turbulent flows, the difference in $G^\star$ in the RKSSP(2,5) and RKC(5), $\epsilon = 0.15$ is fairly dramatic.

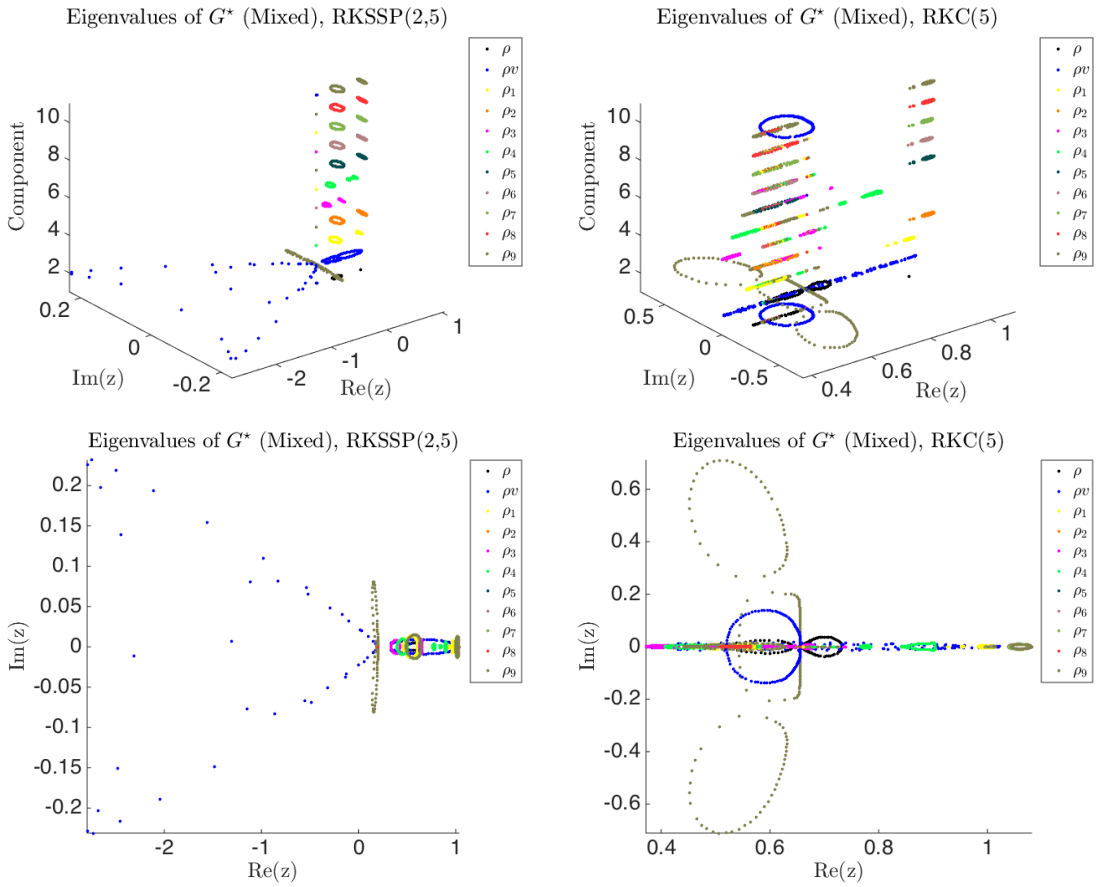

Figure 12: The fully mixed regime $\mathscr{R}^{\mathcal{L}}_{\mathcal{I}}$ from Fig. 3 shows complicated spectral behavior in $G^\star$.

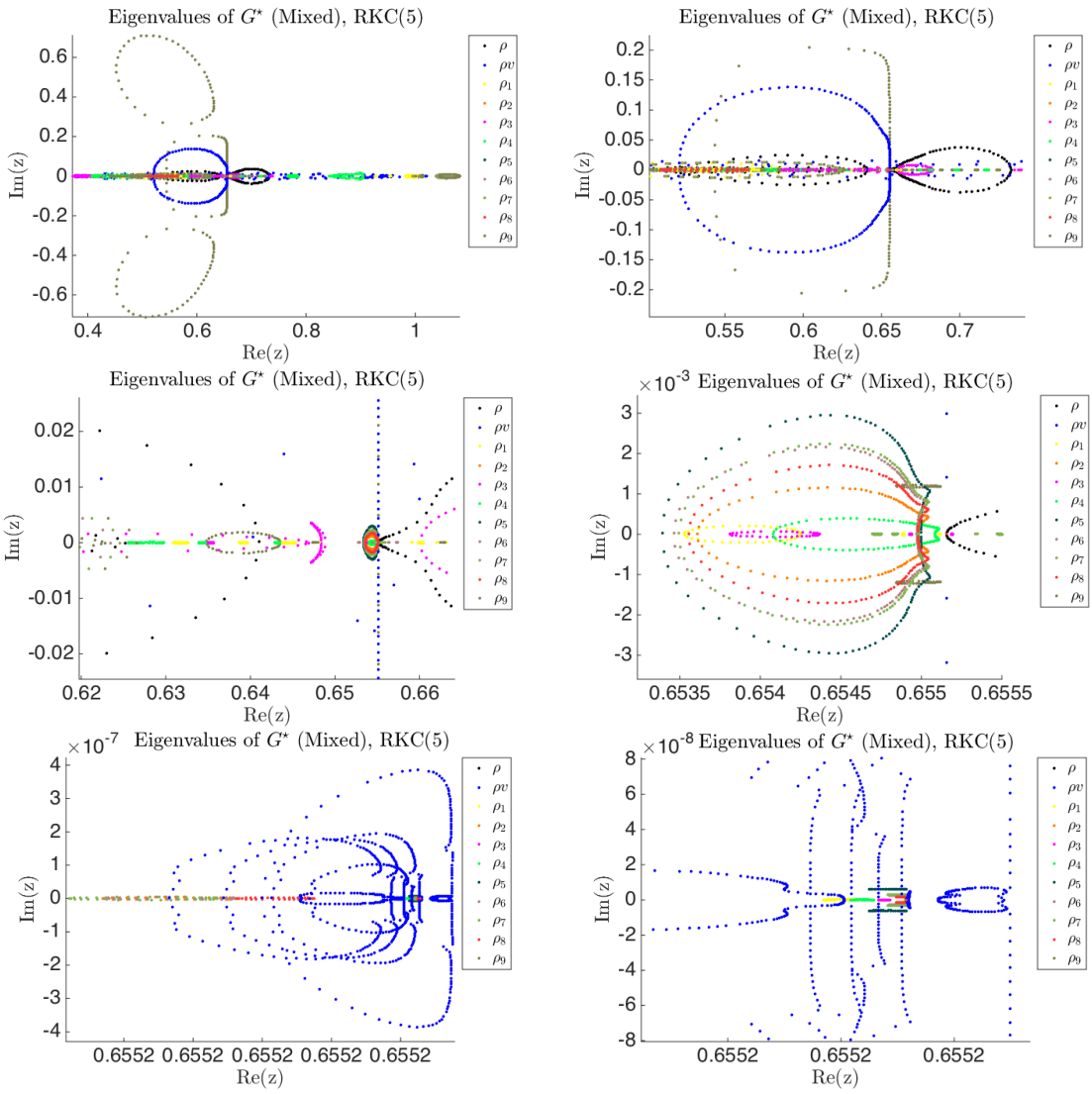

Figure 13: For the mixed problem showing $G^\star$, with $dt = h/18$, for RKC(5), $\epsilon = 0.15$, show increasing zooms of the spectrum.

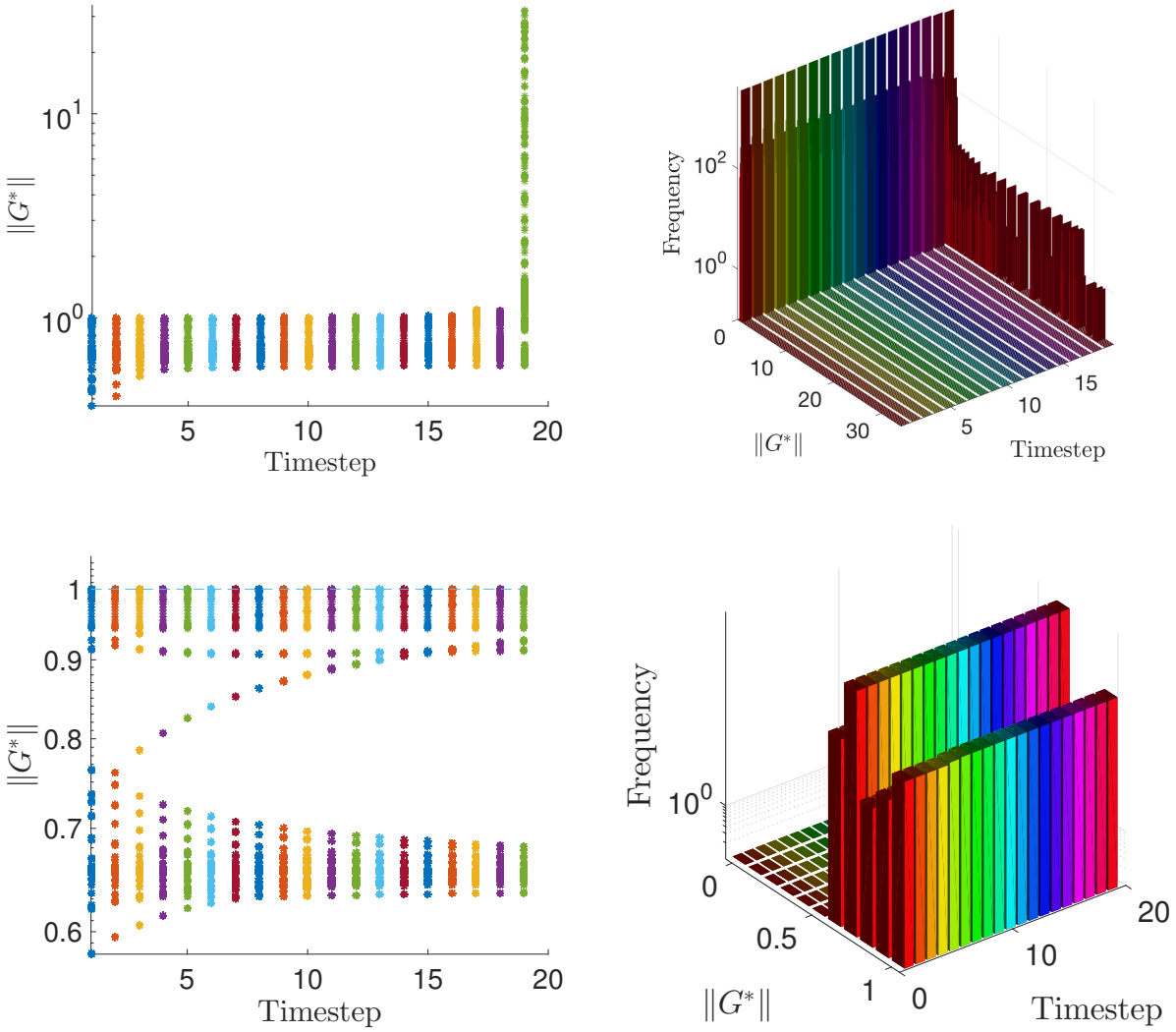

Figure 14: Top row shows the values of $\|G^*\|$ over the time steps 1–19 and its corresponding histogram for the unstable $\Delta t = h/20$, and the bottom row shows the corresponding values of $\|G^*\|$ for the stable case $\Delta t = h/100$.

more complicated eigenstructure, though the presence of this additional structure does not seem to simultaneously suggest anything about the stability features of the solution, and small instabilities in RKC seem to be more numerically robust that in RKSSP tests. Indeed, dividing the timestep by a larger factor, $dt = h/45$ is enough to stabilize both schemes, and leads to similar results as those above, where the RKC scheme is stable with a more elaborate spectrum, and the RKSSP scheme is stable with a less elaborate spectrum. What is remarkable in these nonlinear systems, however, is the incredible nested complexity in the spectrum. For example, a typical set of zooms is shown in Fig. 13 for the fully mixed regime, where nested self-similarity and nonlinear coupling in the spectrum seems to indicate a wealth of complicated dynamics present in the solution space.

Note that an essential observation of Section 3.2 is that even after partially linearizing the nonlinear system, the eigenspectrum bound is not sufficient for stability, which is in contrast to that of the classical linear von Neumann analysis. Rather for DG systems governed by (1.2), under the partial linearization assumption, it is the bound on the spectral norm $\|G^{\star}_{ij}(t^n)\| \leq 1$ that ultimately determines stability. To illustrate this behavior we again show the results from the mixed regime detailed in Fig. 13, but now give the results in a strictly stable regime, $\Delta t = h/45$, and a regime that becomes rapidly unstable $\Delta t = h/20$. As can be seen from Fig. 14, the spectral norm captures this behavior as expected.

The first question that these numerical experiments on the nonlinear stability behavior of the various regimes governed by (1.2) raises is: is it ultimately the truncation of the thicker region or the inclusion of partial modes from the thinner region that dominate the stability behavior in RKC or RKSSP schemes? Unfortunately the answer to this question seems to be ambiguous, and to depend largely on the specifics of the problem at hand. Moreover, the natural follow-up question then becomes: how substantially do the dynamics (and thus the accuracy) of the problem get perturbed relative to the various regimes when choosing thick versus thin region stability schemes? As a general rule, the answer to this problem too seems to be ambiguous. What can be said with confidence, however, is that nonlinear convection-diffusion-reaction systems of the form (1.2) can demonstrate very complicated, highly internally coupled eigenspectra, to such an extent that choosing a temporal discretization scheme without determining the corresponding stability can lead to unpredictable, and potentially spurious numerical results.

Some additional intuition however can also be shared, with regards to the behavior of RKC versus RKSSP schemes in these nonlinear regimes. After exhaustive testing, it can be suggested that, at least up to the nonlinear system studied in Section 5, convection-dominated type flows seem to be fairly well-suited for being stabilized by RKSSP schemes. It seems that these types of flows in general tend to be dominated by fairly thick stability regions. In contrast, diffusive, turbulent, and reaction dominated flows (and thus flows with nonlinear source terms as well) seem to demonstrate more erratic behaviors, where thin-region stability can completely dominate the behavior. The degree to which this occurs, particularly with diffusion-domninated type flows, seems to depend strongly on the form the nonlinear operator takes. As a consequence, it seems reasonable to suggest that in the presence of nonlinear diffusion, reaction and/or source terms, RKC methods might be the most efficient choice for temporal stabilization. However, these suggestions should be taken with caution, as neither case is cut-and-dry, and even in the simple cases explored in Section 5, we have observed counterexamples to both of these "rules of thumb." It may be that in mixed regimes, alternating (both spatially and temporally) between RKC and RKSSP could be an efficient way of managing when different aspects of the flow dominate in different regimes locally.

6 Conclusion

In this paper we have introduced a framework for nonlinear stability analysis using an analogue to classical von Neumann analysis in the context of discontinuous Galerkin methods applied to generalized systems of convection-diffusion-reaction equations (1.2). Our results indicate that a sufficient condition for assuring stability of a method in this context, is to simply guarantee that the *discrete nonlinear stability condition* from Section 3.3 is satisfied.

We examined the reactive Navier-Stokes equations applied to a problem arising in atmospheric chemistry, and performed extensive numerical tests, where we studied the stability of the problem in different regimes as listed in Fig. 3. We closely examined the effect of the so-called "thin region stability" temporal discretizations (i.e. RKC schemes), versus strong stability preserving discretizations (i.e. RKSSP schemes) to see how the stability behavior of the nonlinear system changed under each. The results indicate that when the *discrete nonlinear stability condition* is satisfied, both schemes are stable, though consistently RKC schemes lead to more elaborate eigenspectra than RKSSP schemes. The precise effect this has on instability and accuracy, however, is not entirely clear, and remains an open and interesting question for future analysis.

7 Acknowledgements

Clint Dawson and Craig Michoski would like to acknowledge the support of the National Science Foundation grant ACI-1339801. Ethan Kubatko would like to aknowledge support of the National Science Foundation grant DMS-1217218.

8 Appendix

8.1 Computation of the $G^\star$ Operator:

In this section we briefly outline the definition of the operators appearing in an RK scheme. Note that at the ith stage of an RK scheme we can write $\boldsymbol{u}^{(i)} = G_i u^{(0)}$ where G_i is an ith degree polynomial. Identifying the G_i polynomials with the s-vectors of their coefficients, we have for the RKSSP scheme:

$$G_0 = (1, 0, \cdots, 0)^T, \quad G_1 = (0, 1, 0, \cdots, 0)^T,$$

and for $2 \leq i \leq s$,

$$G_{i,k} = \begin{cases} \sum_{l=0}^{i-1} \alpha_{i-1,l} G_{l,0} - \frac{\alpha_{0,0}}{\beta_{0,0}} \beta_{i-1,l} G_{l,0} & \text{for } k = 0, \\ \sum_{l=0}^{i-1} [\alpha_{i-1,l} G_{l,k} - \frac{a_{0,0}}{\beta_{0,0}} \beta_{i-1,l} G_{l,0} + \frac{1}{\beta_{1,1}} \beta_{i-1,l} G_{l,k-1}] & \text{for } 2 \leq k \leq i, \\ 0 & \text{for } i+1 \leq k \leq s. \end{cases} \tag{8.1}$$

For the RKC scheme we have,

$$G_{i,k} = \begin{cases} (1-\mu_i-\nu_i) + \mu_i G_{i-1,0} + \nu_i G_{i-2,0} - \dfrac{1}{\tilde{\mu}_1}(\tilde{\mu}_i G_{i-1,0} + \tilde{\gamma}_i) & \text{for } k = 0, \\ \mu_i G_{i-1,1} + \nu_i G_{i-2,1} + \dfrac{1}{\tilde{\mu}_1}(\tilde{\gamma}_i + \tilde{\mu}_i G_{i-1,0} - \tilde{\mu}_i G_{i-1,1}) & \text{for } k = 1, \\ \mu_i G_{i-1,k} + \nu_i G_{i-2,k} + \dfrac{1}{\tilde{\mu}_1}(\tilde{\mu}_i G_{i-1,k-1} - \tilde{\mu}_i G_{i-1,k}) & \text{for } 2 \le k \le i, \\ 0 & \text{for } i+1 \le k \le s. \end{cases} \tag{8.2}$$

Finally, we use $G^\star = G_s$ as the definition of the $G^\star$ operator.

8.2 Simple illustrative example: Burger's equation

Consider the one-dimensional Burger's equation

$$u_t + \frac{1}{2}(u^2)_x = 0,$$

with periodic boundary data. The weak form of such a system satisfies (2.7), such that:

$$\frac{d}{dt}\int_{\Omega_{e_i}} \varphi_h u_h \, dx = F_i - \int_{\Omega_{e_i}} f(u_h)\partial_x \varphi_h \, dx. \tag{8.3}$$

Note here that $f = u^2/2$.

Now, to proceed a numerical flux is specified that is associated to F_i. For illustration, let us choose the local Lax-Friedrich's flux

$$\hat{f}_{\text{LLF}} = \frac{1}{2}(f|_{\Gamma_{i\ell}} + f|_{\Gamma_{\ell i}} - \alpha(u_h|_{\Gamma_{i\ell}} - u_h|_{\Gamma_{\ell i}}),$$

such that,

$$F_i = \sum_{\ell \in \Xi(i)} \int_{\Gamma_{i\ell}} (\hat{f}_{\text{LLF}})_{i\ell} \varphi_h|_{\Gamma_{i\ell}} n dS.$$

Now that the flux has been specified, we proceed with the partial linearization from (3.3). The first step in doing so is to rewrite the representation with respect to the lth degree of freedom and replace f with the partial linearization in the volume integral, such that:

$$\frac{d}{dt}u_l^i(t) = \frac{2l+1}{h}\left\{ F_{il} - \int_{\Omega_{e_i}} (J_u f) u_h \partial_x \varphi_l(x) \, dx \right\}. \tag{8.4}$$

Next the partial linearization is performed on the flux representations, such that:

$$F_{il} = \frac{1}{2}\sum_{\ell \in \Xi(i)} \int_{\Gamma_{i\ell}} \left(f|_{\Gamma_{i\ell}} + f|_{\Gamma_{\ell i}} - \alpha(u_h|_{\Gamma_{i\ell}} - u_h|_{\Gamma_{\ell i}})\right) n_{i\ell} \varphi_l dS,$$

where the Jacobian in this case is trivially $(J_u f)|_{\Gamma_{i\ell}} = u_h|_{\Gamma_{i\ell}}$, and $\alpha = \max(u_h|_{\Gamma_{i\ell}}, u_h|_{\Gamma_{\ell i}})$. This means we now have the system:

$$\begin{aligned} \frac{d}{dt}u_l^i = \frac{2l+1}{h}\Bigg\{ \frac{1}{2}\sum_{\ell \in \Xi(i)} \int_{\Gamma_{i\ell}} & ([(J_u f)u_h]|_{\Gamma_{i\ell}} + [(J_u f)u_h]|_{\Gamma_{\ell i}} - \alpha(u_h|_{\Gamma_{i\ell}} - u_h|_{\Gamma_{\ell i}}))\varphi_l n_{i\ell} dS \\ & - \int_{\Omega_{e_i}} (J_u f) u_h \partial_x \varphi_l(x) \, dx \Bigg\}, \end{aligned} \tag{8.5}$$

so that using the same argument from Section 3.1, the flux can now be split relative to contributions determined by the stencil generated by cell "ownership," as in (3.4).

To make this explicit, let us consider only the flux contribution,

$$\frac{2l+1}{2h}\sum_{\ell\in\Xi(i)}\int_{\Gamma_{i\ell}}([(J_uf)u_h]|_{\Gamma_{i\ell}}+[(J_uf)u_h]|_{\Gamma_{\ell i}}-\alpha(u_h|_{\Gamma_{i\ell}}-u_h|_{\Gamma_{\ell i}}))\varphi_l n_{i\ell}dS.$$

This term is rewritten relative to cell ownership, such that:

$$\frac{2l+1}{2h}\left(\sum_{k,m}^{n_p}F'_{km}u_m\varphi_l\right)\Big|_{\Gamma_{i\ell}}+\frac{2l+1}{2h}\left(\sum_{k,m}^{n_p}F'_{km}u_m\varphi_l\right)\Big|_{\Gamma_{\ell i}}=$$
$$\left(\frac{2l+1}{2h}\sum_{\ell\in\Xi(i)}\int_{\Gamma_{i\ell}}(J_uf|_{\Gamma_{i\ell}}-\alpha)u_h|_{\Gamma_{i\ell}}\varphi_l n_{i\ell}dS\right)+\left(\frac{2l+1}{2h}\sum_{\ell\in\Xi(i)}\int_{\Gamma_{\ell i}}(J_uf|_{\Gamma_{\ell i}}+\alpha)u_h|_{\Gamma_{\ell i}}\varphi_l n_{i\ell}dS\right).$$

This makes it clear now that the F'_{km} denotes an evaluated form of $J_uf+\alpha$.

As stated in Section 3.1, F'_{jkm} is an $N\times(n_p+1)^2$ tensor, meaning for a single component flow such as Burger's, we have that F'_{km} is a $(n_p+1)\times(n_p+1)$ matrix, in this case defined by:

$$F'_{km}=\sum_{\ell\in\Xi(i)}\int_{\Gamma_{i\ell}}(J_uf|_{\Gamma_{i\ell}}+\alpha)_k\varphi_m n_{i\ell}dS.$$

To see this we recognize that $(J_uf)=u_h=\sum_{l=0}^{n_p}u_l\varphi_l$ is a vector of length n_p+1, as is α. Thus simply factoring out the basis function from the solution, and evaluating at the support points yields:

$$\begin{aligned}&\left(\frac{2l+1}{2h}\sum_{\ell\in\Xi(i)}\int_{\Gamma_{i\ell}}(J_uf|_{\Gamma_{i\ell}}-\alpha)u_h|_{\Gamma_{i\ell}}\varphi_l n_{i\ell}dS\right)+\left(\frac{2l+1}{2h}\sum_{\ell\in\Xi(i)}\int_{\Gamma_{i\ell}}(J_uf|_{\Gamma_{\ell i}}+\alpha)u_h|_{\Gamma_{\ell i}}\varphi_l n_{i\ell}dS\right)\\&\quad=\left(\frac{2l+1}{2h}\sum_{\ell\in\Xi(i)}\sum_{k,m}^{n_q}\int_{\Gamma_{i\ell}}(J_uf|_{\Gamma_{i\ell}}-\alpha)_k(\varphi_m u_m)|_{\Gamma_{i\ell}}\varphi_l n_{i\ell}dS\right)\\&\qquad+\left(\frac{2l+1}{2h}\sum_{\ell\in\Xi(i)}\sum_{k,m}^{n_q}\int_{\Gamma_{\ell i}}(J_uf|_{\Gamma_{\ell i}}+\alpha)_k(\varphi_m u_m)|_{\Gamma_{\ell i}}\varphi_l n_{i\ell}dS\right).\end{aligned}\tag{8.6}$$

Notice that (8.5), after substituting the explicit form (8.6) in for the surface terms, comprise the matrices in (3.11) that end up forming the G_j matrix from (3.12).

The factored contribution F'_{km}, being an $(n_p+1)\times(n_p+1)$ matrix, clearly has dependencies on the degrees of freedom (e.g. the spatial nodes) of the cell that owns it. However, the assumption of the partial linearization (3.2) is that within the cell distance $\Delta x<h$, these spatial dependencies can be decoupled (by scaling arguments) from the dependencies in the Fourier expansion and subsequent shift. Numerical examples seem to reinforce the validity of this assumption.

References

[1] H. Ammari. *Modeling and computations in electromagnetics: a volume dedicated to Jean-Claude Nedelec*. Lecture Notes in Computational Science and Engineering. Springer, Dordrecht, 2007.

[2] D. Arnold, F. Brezzi, B. Cockburn, and D. Marini. Discontinuous Galerkin methods for elliptic problems. In *Discontinuous Galerkin methods (Newport, RI, 1999)*, volume 11 of *Lect. Notes Comput. Sci. Eng.*, pages 89–101. Springer, Berlin, 2000.

[3] D. N. Arnold, F. Brezzi, B. Cockburn, and L. D. Marini. Unified analysis of discontinuous Galerkin methods for elliptic problems. *SIAM J. Numer. Anal.*, 39(5):1749–1779, 2001/02.

[4] K. E. Atkinson. *An introduction to numerical analysis*. John Wiley & Sons, Inc., New York, second edition, 1989.

[5] R. Atkinson, D. L. Baulch, R. A. Cox, J. N. Crowley, R. F. Hampson, R. G. Hynes, M. E. Jenkin, M. J. Rossi, J. Troe, and T. J. Wallington. Evaluated kinetic and photochemical data for atmospheric chemistry: Volume IV - gas phase reactions of organic halogen species. *Atmospheric Chemistry and Physics*, 8(15):4141–4496, 2008.

[6] S. Chapman and T. G. Cowling. *The mathematical theory of nonuniform gases*. Cambridge Mathematical Library. Cambridge University Press, Cambridge, third edition, 1990. An account of the kinetic theory of viscosity, thermal conduction and diffusion in gases, In co-operation with D. Burnett, With a foreword by Carlo Cercignani.

[7] C. Dawson, J. Westerink, J. Feyen, and D. Pothina. Continuous, discontinuous and coupled discontinuous-continuous Galerkin finite element methods for the shallow water equations. *Internatioanl Journal for Numerical Methods in Fluids*, 52(1):63–88, Sep 10 2006.

[8] S. Descombes and M. Massot. Operator splitting for nonlinear reaction-diffusion systems with an entropic structure: singular perturbation and order reduction. *Numer. Math.*, 97(4):667–698, 2004.

[9] E. Feireisl, A. Novotný, and H. Petzeltová. On the domain dependence of solutions to the compressible Navier-Stokes equations of a barotropic fluid. *Math. Methods Appl. Sci.*, 25(12):1045–1073, 2002.

[10] R. Fitzpatrick and F. Waelbroeck. Two-fluid magnetic island dynamics in slab geometry. ii. islands interacting with resistive walls or resonant magnetic perturbations. *Physics of Plasmas*, 12(2), 2005.

[11] V. Giovangigli. *Multicomponent flow modeling*. Modeling and Simulation in Science, Engineering and Technology. Birkhäuser Boston Inc., Boston, MA, 1999.

[12] S. Gottlieb, D. Ketcheson, and C.-W. Shu. High order strong stability preserving time discretizations. *Journal of Scientific Computing*, 38(3):251–289, 2009.

[13] S. Gottlieb, C.-W. Shu, and E. Tadmor. Strong stability-preserving high-order time discretization methods. *SIAM Rev.*, 43(1):89–112 (electronic), 2001.

[14] R. E. Heath, I. M. Gamba, P. J. Morrison, and C. Michler. A discontinuous Galerkin method for the Vlasov-Poisson system. *Journal of Computational Physics*, 231(4):1140–1174, Feb 20 2012.

[15] J. Hirschfelder, C. Curtiss, and R. Bird. *The Molecular Theory of Gases and Liquids*. Structure of Matter Series. Wiley-Interscience, Revised, New York, 1954.

[16] N. N. Janenko. The method of fractional steps for the solution of problems in continuum mechanics. In *Partial differential equations (Proc. Sympos.) (Russian)*, pages 239–249. Izdat. "Nauka", Moscow, 1970.

[17] E. Kubatko, C. Dawson, and J. Westerink. Time step restrictions for Runge-Kutta discontinuous Galerkin methods on triangular grids. *J. Comput. Phys.*, 227(23):9697–9710, 2008.

[18] E. Kubatko, J. Westerink, and C. Dawson. An unstructured grid morphodynamic model with a discontinuous Galerkin method for bed evolution. *Ocean Modelling*, 15(1-2):71–89, 2006. 3rd International Workshop on Unstructured Mesh Numerical Modelling of Coastal, Shelf and Ocean Flows, Toulouse, France, SEP 20-22, 2004.

[19] E. Kubatko, J. Westerink, and C. Dawson. Semi discrete discontinuous Galerkin methods and stage-exceeding-order, strong-stability-preserving Runge-Kutta time discretizations. *J. Comput. Phys.*, 222(2):832–848, 2007.

[20] E. Kubatko, B. Yeager, and D. Ketcheson. Optimal Strong-Stability-Preserving Runge-Kutta Time Discretizations for Discontinuous Galerkin Methods. *Journal of Scientific Computing*, 60(2):313–344, 2014.

[21] R. LeVeque. *Finite Difference Methods for Ordinary and Partial Differential Equations: Steady-State and Time-Dependent Problems (Classics in Applied Mathematics Classics in Applied Mathemat)*. Society for Industrial and Applied Mathematics, Philadelphia, PA, USA, 2007.

[22] H. Liu and H. Yu. The Entropy Satisfying Discontinuous Galerkin Method for Fokker-Planck equations. *Journal of Scientific Computing*, 62(3):803–830, Mar 2015.

[23] X. Liu and Q. Nie. Compact integration factor methods for complex domains and adaptive mesh refinement. *J. Comput. Phys.*, 229(16):5692–5706, 2010.

[24] J. Loverich, A. Hakim, and U. Shumlak. A Discontinuous Galerkin Method for Ideal Two-Fluid Plasma Equations. *Communications in Computational Physics*, 9(2):240–268, Feb 2011.

[25] B. Lu and Y. C. Zhou. Poisson-Nernst-Planck Equations for Simulating Biomolecular Diffusion-Reaction Processes II: Size Effects on Ionic Distributions and Diffusion-Reaction Rates. *Biophysical Journal*, 100(10):2475–2485, MAY 18 2011.

[26] A. Mellet and A. Vasseur. On the barotropic compressible Navier-Stokes equations. *Comm. Partial Differential Equations*, 32(1-3):431–452, 2007.

[27] C. Michoski, J. Evans, and P. Schmitz. Discontinuous galerkin -adaptive methods for multiscale chemical reactors: Quiescent reactors. *Computer Methods in Applied Mechanics and Engineering*, 279(0):163 – 197, 2014.

[28] C. Michoski and A. Vasseur. Existence and uniqueness of strong solutions for a compressible multiphase Navier-Stokes miscible fluid-flow problem in dimension n = 1. *Mathematical Models and Methods in Applied Sciences*, 19(03):443–476, 2009.

[29] G. Naldi, L. Pareschi, and G. Toscani, editors. *Mathematical Modeling of Collective Behavior in Socio-Economic and Life Sciences*. Birkhäuser Boston, Boston, 2010.

[30] D. L. Ropp and J. N. Shadid. Stability of operator splitting methods for systems with indefinite operators: reaction-diffusion systems. *J. Comput. Phys.*, 203(2):449–466, 2005.

[31] D. L. Ropp and J. N. Shadid. Stability of operator splitting methods for systems with indefinite operators: advection-diffusion-reaction systems. *J. Comput. Phys.*, 228(9):3508–3516, 2009.

[32] S. Ruuth. Global optimization of explicit strong-stability-preserving Runge-Kutta methods. *Math. Comp.*, 75(253):183–207 (electronic), 2006.

[33] C.-W. Shu and S. Osher. Efficient implementation of essentially nonoscillatory shock-capturing schemes. *J. Comput. Phys.*, 77(2):439–471, 1988.

[34] J. Smoller. *Shock waves and reaction-diffusion equations*, volume 258 of *Grundlehren der Mathematischen Wissenschaften [Fundamental Principles of Mathematical Sciences]*. Springer-Verlag, New York, second edition, 1994.

[35] V. A. Solonnikov and A. Tani. Evolution free boundary problem for equations of motion of viscous compressible barotropic liquid. In *The Navier-Stokes equations II—theory and numerical methods (Oberwolfach, 1991)*, volume 1530 of *Lecture Notes in Math.*, pages 30–55. Springer, Berlin, 1992.

[36] B. Sportisse. An analysis of operator splitting techniques in the stiff case. *J. Comput. Phys.*, 161(1):140–168, 2000.

[37] B. Srinivasan, A. Hakim, and U. Shumlak. Numerical Methods for Two-Fluid Dispersive Fast MHD Phenomena. *Communications in Computational Physics*, 10(1):183–215, Jul 2011.

[38] J. C. Strikwerda. *Finite difference schemes and partial differential equations*. Society for Industrial and Applied Mathematics (SIAM), Philadelphia, PA, second edition, 2004.

[39] J. Sutherland and C. Kennedy. Improved boundary conditions for viscous, reacting, compressible flows. *J. Comput. Phys.*, 191:502–524, 2003.

[40] M. Tabei, T. Mast, and R. Waag. A k-space method for coupled first-order acoustic propagation equations. *Journal of the Acoustical Society of America*, 111(1, 1):53–63, JAN 2002.

[41] M. Torrilhon and R. Jeltsch. Essentially optimal explicit Runge-Kutta methods with application to hyperbolic-parabolic equations. *Numer. Math.*, 106(2):303–334, 2007.

[42] L. N. Trefethen. Finite difference and spectral methods for ordinary and partial differential equations, 1996.

[43] P. J. van Der Houwen and B. P. Sommeijer. On the internal stability of explicit, m-stage runge-kutta methods for large m-values. *ZAMM - Journal of Applied Mathematics and Mechanics / Zeitschrift fÃijr Angewandte Mathematik und Mechanik*, 60(10):479–485, 1980.

[44] J. G. Verwer and B. P. Sommeijer. An implicit-explicit Runge-Kutta-Chebyshev scheme for diffusion-reaction equations. *SIAM J. Sci. Comput.*, 25(5):1824–1835 (electronic), 2004.

[45] F.-B. Wang. A PDE system modeling the competition and inhibition of harmful algae with seasonal variations. *Nonlinear Analysis: Real World Applications*, 25(0):258 – 275, 2015.

[46] G. Wanner, E. Hairer, and S. Norsett. Order stars and stability theorems. *BIT Numerical Mathematics*, 18(4):475–489, 1978.

[47] N. Wiebe, D. Berry, P. Høyer, and B. C. Sanders. Higher order decompositions of ordered operator exponentials. *Journal of Physics A: Mathematical and Theoretical*, 43(6):065203, 2010.

[48] F. Wu and R. W. Carr. Kinetics of CH2ClO radical reactions with O2 and NO, and the unimolecular elimination of HCl. *The Journal of Physical Chemistry A*, 105(9):1423–1432, 2001.